Environmental Science and Ecotechnology 21 (2024) 100429

Contents lists available at ScienceDirect

Environmental Science and Ecotechnology

journal homepage: www.journals.elsevier.com/environmental-science-and-ecotechnology/

Review

Solute flow and particle transport in aquatic ecosystems: A review on the effect of emergent and rigid vegetation

Judy Q. Yang

St. Anthony Falls Laboratory, Department of Civil, Environmental, and Geo-Engineering, University of Minnesota Twin Cities, MN, USA

ARTICLE INFO

Article history:
Received 5 September 2023
Received in revised form
8 May 2024
Accepted 8 May 2024

ABSTRACT

In-channel vegetation is ubiquitous in aquatic environments and plays a critical role in the fate and transport of solutes and particles in aquatic ecosystems. Recent studies have advanced our understanding of the role of vegetation in solute flow and particle transport in aquatic ecosystems. This review summarizes these papers and discusses the impacts of emergent and rigid vegetation on the surface flow, the advection and dispersion of solutes, suspended load transport, bedload transport, and hyporheic exchange. The two competing effects of emergent vegetation on the above transport processes are discussed. On the one hand, emergent vegetation reduces mean flow velocity at the same surface slope, which reduces mass transport. On the other hand, at the same mean flow velocity, vegetation generates turbulence, which enhances mass transport. Mechanistic understanding of these two competing effects and predictive equations derived from laboratory experiments are discussed. Predictive equations for the mean flow velocity and turbulent kinetic energy inside an emergent vegetation canopy are derived based on force and energy balance. The impacts of emergent vegetation on the advection-dispersion process, the suspended load and bedload transport, and the hyporheic exchange are summarized. The impacts of other vegetation-related factors, such as vegetation morphology, submergence, and flexibility, are briefly discussed. The role of vegetation in transporting other particles, such as micro- and macro-plastics, is also briefly discussed. Finally, suggestions for future research directions are proposed to advance the understanding of the dynamic interplays among natural vegetation, flow dynamics, and sedimentary processes.

1. Introduction

The transport of solutes and particles in water plays an essential role in the health and stability of aquatic habitats, including rivers, lakes, estuaries, and coasts. Soluble nutrients, such as essential ions and dissolved organic matter, are crucial for the survival and proliferation of aquatic organisms [1,2]. Although essential, excessive nutrients like phosphate can lead to significant environmental issues, such as harmful algal blooms [3]. Synthetic solutes such as agricultural and pharmaceutical products have been found in many aquatic environments, posing potential threats to aquatic organisms and human health [4,5]. The concentration of these solutes, which consequently determines their impacts on the metabolism and health of aquatic environments, is regulated by their transport in the surface water and the hyporheic zone [6,7], or the sediment region where mixing of surface and subsurface water occurs [7]. A fundamental understanding of the fate and transport of solutes can help ecologists design strategies to ensure sufficient but not excess nutrients in aquatic habitats and prevent contamination.

In addition to solutes, sediment and particulate organic matter are essential to aquatic environments. Sediment constitutes the beds/bottoms and banks of aquatic environments. Moderate sediment erosion can create habitats for some animals, such as macroinvertebrates requiring coarse sediment for oxygenation [8]. Excess erosion can demobilize habitats, adversely affecting inhibited biological organisms' abundance and diversity [9,10]. Fine sediment particles can also suspend in the water column, reducing visibility, smothering fishes, and irritating the digestive systems of fishes and other aquatic animals [11–13]. Fine sediment, characterized by electrochemically active surfaces [14], adsorbs abundant nutrients [15,16], heavy metals [17,18], organic contaminants such as pesticides [19,20], and pathogens [21,22]. Consequently, fine sediment transport, a carrier of nutrients and contaminants,

E-mail address: judyyang@umn.edu.

https://doi.org/10.1016/j.ese.2024.100429

significantly impacts the biogeochemical cycle [23] and contaminant dispersion [24–26] in aquatic ecosystems. Furthermore, particulate organic matter and pollutant particles are widely present in aquatic environments [27,28]. Particulate organic carbon transport is crucial to the global carbon cycle [29]. The transport of pollutant particles, such as microplastics (<5 mm) and macroplastics (≥5 mm), poses a threat to human health and biodiversity [30]. Understanding sediment and particle fate and transport is essential for strategies to restore eroded habitats and prevent contamination spread.

Vegetation, a common component of natural aquatic environments, impacts the transport of solutes and particles in surface water and hyporheic exchange [31–35]. Vegetation can both slow surface flow by creating drag, reducing mass transport [36–39], and enhance solute dispersion and suspended and bedload transport by generating turbulence [40–42]. The net impact of vegetation on mass transport results from the dominance of either drag reduction or turbulence enhancement [42–45] (Fig. 1). In addition to surface water, vegetation has been shown to impact the exchange of solutes and particles between surface water and subsurface water in the hyporheic zone [33,46–48]. Such impacts can be attributed to the vegetation-induced pressure gradient at the scale of vegetation stem size [48,49], the vegetation-generated turbulence [33], and the vegetation-induced pressure gradient at the patch scale. Understanding these mechanisms' roles in solute and particle transport regulation is crucial for preserving and restoring the stability and health of aquatic ecosystems with vegetation.

This review explores how emergent and rigid vegetation impacts the transport of solutes and particles in the surface water and the hyporheic zone. Section two outlines vegetation-characterizing parameters. Section three discusses the impacts of vegetation on the mean surface flow velocity, turbulent kinetic energy, and dispersion of solutes. Section four addresses the impacts of vegetation on sediment transport, including suspended load and bedload. Section five delves into current insights into vegetation's role in hyporheic exchange. Section six discusses the impacts of other vegetation-related factors, such as vegetation morphology, submergence, and flexibility, on the flow and mass transport. This section also proposes future research directions.

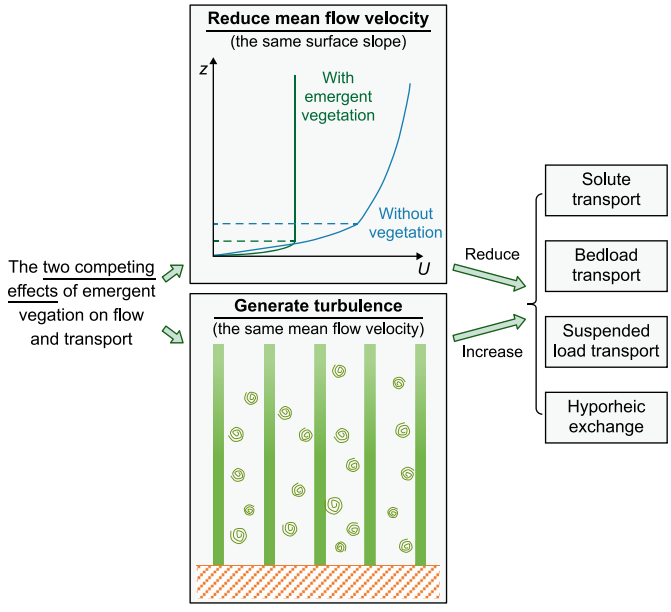

Fig. 1. Overview of the two competing effects of emergent and rigid vegetation (green cylinders) on fluid flow and mass transport. On the one hand, at the same water surface or energy slope, vegetation reduces the mean surface flow velocity U, reducing solute transport, bedload transport, suspended load transport, and hyporheic exchange. On the other hand, at the same mean flow velocity U, vegetation generates additional turbulence (the green eddies), leading to increases in solute transport, bedload and suspended load transport, and hyporheic exchange. Both effects need to be considered to quantify the net effect of emergent vegetation on mass transport.

2. Characterization of vegetation

Aquatic vegetation, also called aquatic macrophytes and plants, is widely present in freshwater and saltwater ecosystems [31,50–52]. According to their relative size and position compared to the water depth, vegetation can be categorized into three types [53]: submerged, emergent, and floating. Submerged vegetation, such as *Zosteraceae* (seagrass), has a height h_v less than the water depth h; emergent vegetation, such as *Spartina alterniflora*, protrudes through the water surface and has a height h_v larger than h; floating vegetation, such as *Lemnoideae* (duckweeds), which does not attach to the sediment and only occupy part of the water column, has an in-water height h_v smaller than h. In addition to the relationship between vegetation height and water depth, vegetation can be categorized based on its rigidity as flexible and rigid [54]. Many salt marsh plants, such as *Spartina alterniflora,* have limited bending in their regular flow environments and are modeled as rigid vegetation [36,55]. A schematic diagram of the emergent submerged and floating vegetation is shown in Fig. A1 (in the Supplementary Materials). A glossary of key parameters discussed in this review is listed in Table A1.

In many mathematical models, vegetation stems are often simplified as cylinders with diameter d_v or thin blades with width l_a and thickness l_b, despite the vertical variation of the shape of vegetation stems [31,36,56–60]. Vegetation stems form patches or canopies of various shapes, including rectangular or circular shapes [60–62]. The density of vegetation inside the canopy can be characterized by the number of vegetation stems per unit bed area n (m^{-2}), vegetation volume fraction φ (unitless), and vegetation frontal area per unit volume a (m^{-1}). The vegetation volume fraction is defined as the volume of vegetation divided by the total volume of water and vegetation. For cylindrical and emergent vegetation $\varphi = \frac{\pi}{4} n d_v^2$; for blade-like emergent vegetation $\varphi = n l_a l_b$ [31]. The vegetation frontal area per unit volume a, which is often referred to as vegetation density, is equal to the total frontal area of vegetation stems (the area that is blocking the flow) divided by the total volume (water + vegetation volume) [36]. For cylindrical and rigid emergent vegetation, $a = n d_v$ and $\varphi = \frac{\pi}{4} a d_v$. This review summarizes results from laboratory studies using emergent and rigid cylindrical vegetation [36,57–60,62,63], such as wood or aluminum cylinders. This simplified vegetation model allows high-resolution measurements of the flow and mass transport inside the vegetation patch in a water-recirculating flume under systematically controlled flow conditions. Many important mechanistic understandings of the role of vegetation in the flow and mass transport are derived from these studies [36,57–59,63]. To apply the equations derived from these studies to the natural environment, other vegetation characteristics also need to be considered, including vegetation morphology, flexibility, submergence, and heterogeneous distribution. The impacts of those factors are discussed in Section 6.

3. Impacts of vegetation on surface flow and solute transport

3.1. Vegetation-generated drag and its impact on the mean flow velocity

When surface water runs through vegetation, it experiences a drag force by the vegetation and slows its velocity. The vegetation-induced drag per fluid mass f_D (m s^{-2}), increases with increasing vegetation frontal area per unit volume a (m^{-1}) and the mean or temporally-averaged flow velocity [36]. For channels without vegetation, the mean bulk flow velocity equals the flow rate Q divided by the cross-sectional area of the channel, which for rectangular channel is $U = \frac{Q}{hl_w}$ with h and l_w denoting the water depth and the channel width, respectively. In channels with emergent vegetation, vegetation reduces the cross-sectional area of the flow and, as such, increases the cross-sectionally-averaged flow velocity at the same Q. To account for such an effect, the spatially-averaged, or volumetrically-averaged, mean velocity is often calculated as $U_p = \frac{U}{(1-\varphi)}$, with the subscript '$p$' denoting pore [39]. In most mathematical models, the vegetation-induced drag per fluid volume is approximated by a quadratic drag law, namely $\rho_D = \frac{1}{2}\rho C_D a U_p^2$, with ρ denoting the fluid density and C_D (on the order of one) denoting the spatially-averaged vegetation drag coefficient [31]. The drag coefficient of an isolated single cylinder, C_{D_single}, has been classically related to the wake structure of the flow and predicted by Re_D, which is the Reynolds number based on the cylinder diameter [64–66], namely $C_{D\_single} = f\left(Re_D = \frac{\rho U_p d_v}{\mu}\right)$, with μ denoting the dynamic viscosity of the fluid. For an array of vegetation, the wake regions of the cylinders interfere with each other when the spacing between vegetation stems is smaller than the length scale of the wake zone; thus, the spatially averaged drag coefficient C_D is also controlled by the spatial arrangement or the density of the vegetation [36].

Many semi-empirical equations have been proposed to predict the spatially-averaged vegetation drag coefficient C_D based on flow velocity and vegetation characteristics such as vegetation volume fraction φ [37,39,67,68]. For example, Tanino and Nepf [39] calculated the C_D of randomly distributed arrays of emergent cylinders based on a combination of velocity and water surface slope measurements. They proposed a semi-empirical equation to predict C_D based on Re_D and vegetation volume fraction φ. The vegetation volume fraction and Reynolds number in their study are in the range of $\varphi = 0.091–0.35$ and $Re_p = \frac{\rho U_p d_v}{\mu} = 25–685$, respectively. Kothyari et al. [69] measured the force on a single cylinder inside a staggered array. They developed another semi-empirical predictive equation for C_D based on φ, Re_D, and Froude number $F = \frac{U_p}{\sqrt{gh}}$. The vegetation volume fraction and Reynolds number in their study [67] are in the range of $\varphi = 0.002–0.089$ and $Re_P = \frac{\rho U_p d_v}{\mu} = 608–2580$, respectively. Cheng and Nguyen [68] calculated C_D from velocity and water surface slope measurements for vegetation volume fraction $\varphi = 0.004–0.12$. They defined a vegetation-related hydraulic radius $r_v = \frac{\pi}{4}\frac{1-\varphi}{\varphi}d_v$ and developed a semi-empirical equation to predict C_D based on $Re_v = \frac{\rho U_p r_v}{\mu}$ and compared their predictions with measurements from several other studies. Etminan et al. [37] calculated C_D of staggered vegetation arrays with $\varphi = 0.0016–0.25$ and $Re_P = 200–1340$ using Large Eddy simulation. They defined a constricted cross-section velocity $U_c = \frac{1-\varphi}{1-\sqrt{2\varphi/\pi}}U_p$ and showed that drag coefficient based on U_c could be predicted by the Reynolds number based on U_c. Some details of the above predictive models of C_D discussed in Refs. [37–39,68–78] are listed in Table 1.

Given the relationship for C_D, the spatially-averaged mean flow velocity U_p inside the vegetation channels can be predicted based on the balance of the driven force due to the water surface slope s, the vegetation drag, and the bed friction force [57], namely

$$\rho g h s = \frac{1}{2}\rho\frac{C_D a}{1-\varphi}hU_p^2 + \rho C_f U_p^2 \quad (1\text{-a})$$

The term on the left-hand side of the equation represents the pressure gradient due to the water surface slope. The first and second terms on the right-hand side of the equations represent the vegetation drag and the bed friction, respectively. This equation can be rearranged to:

$$U_p = \sqrt{\frac{2gs}{C_D a\big/(1-\varphi) + C_f\big/h}} \quad (1\text{-b})$$

where C_f denotes the bed friction coefficient that can be estimated from the sediment size and hydrodynamic properties such as water depth, friction velocity, and Reynolds number [70]. Inside the vegetation, the bed friction drag ($\rho C_f U_p^2$) is often much smaller than the vegetation drag ($\frac{1}{2}\rho\frac{C_D a}{1-\varphi}hU_p^2$) [57]. At the same water surface slope s, the flow velocity U_p in a vegetated channel can be several times to several orders of magnitude smaller than that in a non-vegetated channel. For most vegetated channels with emergent vegetation, the bed friction can be ignored; thus, U_p can be estimated based on a balance of the pressure gradient and the vegetation drag, namely $U_p = \sqrt{\frac{2gs(1-\varphi)}{C_D a}}$.

In addition to altering the spatially-averaged velocity U_p, vegetation alters the vertical distribution of the horizontally-averaged mean flow velocity $\langle\overline{u}\rangle$. The overbar denotes the time average, and the bracket denotes the spatial average of velocity in each horizontal plane. In open channels without vegetation, $\langle\overline{u}\rangle$ can be approximated as a linear or parabolic function of z (the distance from the bed) in the boundary layer close to the bed and a logarithmic function of z above the boundary layer, a distribution often referred to as the law of the wall [70,79] (Fig. 2a, blue curves). In channels with emergent and rigid cylindrical vegetation, the vegetation-generated turbulence mixes fluid, which makes $\langle\overline{u}\rangle$ uniform in the upper water column [36,76]. The distribution of $\langle\overline{u}\rangle$ in the emergent vegetated channel has been approximated by a two-layer model, assuming a parabolic distribution in the boundary layer close to the bed and a uniform distribution above the boundary layer [57,80] (Fig. 2a, green curves). Here the boundary layer refers to the layer close to the bed below the logarithmic and uniform velocity layers.

3.2. Vegetation-induced turbulence

As vegetation slows down the mean flow, its stems extract energy from the mean flow and convert it to turbulent kinetic energy [31,36]. The turbulent kinetic energy represents the instantaneous fluctuations of the flow velocity from the mean. It is defined as $k_t = \frac{(\overline{u'^2}+\overline{v'^2}+\overline{w'^2})}{2}$, with u', v', and w' denoting the instantaneous flow fluctuations from the mean in streamwise, longitudinal, and vertical directions, respectively. The overbar denotes the time average. For turbulent flow ($Re_P > 200$), the energy extracted from the mean flow by the vegetation is mainly through vortex generation in the vegetation wake, and the extracted energy per time, or the rate of work, can be approximated as the vegetation drag times velocity [31,63,81], namely $P_w = \frac{1}{2}C_D a U_p^3$. The extracted energy is mainly

Table 1
A list of several recently-developed equations to predict the spatially-averaged drag coefficient of emergent and rigid cylindrical vegetation array.

Predictive equations for $\overline{C_D}$	Reference	Vegetation characteristics	Range of *Re*	Reference
$C_D = 2\left(\frac{\alpha_0}{Re_p}+\alpha_1\right)$ with coefficients α_0 and α_1 determined by φ	[39] (flume experiments)	Random array, $\varphi = 0.1-0.4$	$Re_P = 5-9\times10^4$	[39] (flume experiments)
$C_D = f(\varphi, Re_p, \xi, F)$ with ξ an order 1 coefficient depends on the vegetation arrangement.	[69] (flume experiments)	Staggered array, $\varphi = 0.002-0.09$	$Re_P = 608-2646$	[69] (flume experiments)
$C_D = \frac{50}{Re_v^{0.43}} + 0.7\left[1-e^{-\frac{Re_v}{15,000}}\right]$	[68] (flume experiments)	Staggered array, $\varphi = 0.004-0.1$	$Re_v = \frac{\rho U_P r_v}{\mu} = 52-5.6\times10^5$	[68] (flume experiments)
$C_{D,c} = 1 = +10Re_c^{-2/3}$ with $C_{D,c}$ and Re_c based on U_c.	[37] (large eddy simulation)	$\varphi = 0.02-0.3$	$Re_P = 200-1340$	[37] (large eddy simulation)

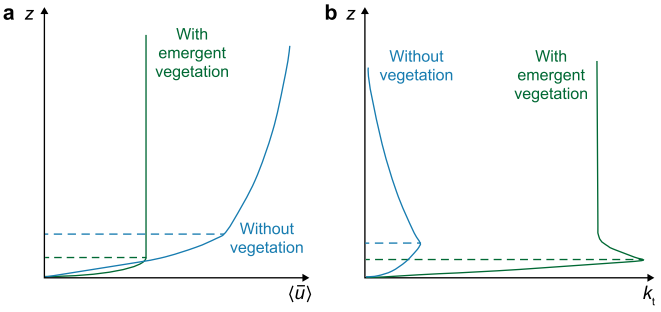

Fig. 2. Schematic diagram showing the impacts of emergent and rigid cylindrical vegetation on the vertical profile of the horizontally-averaged mean flow velocity $\langle\overline{u}\rangle$ and turbulent kinetic energy k_t. The relative magnitude of these variables in the figure does not reflect the actual ratios that vary with vegetation and sediment bed characteristics. **a**, At the same water surface slope, vegetation slows the flow, reduces U_p, and alters the vertical distribution of $\langle\overline{u}\rangle$. Without vegetation, the velocity profile (blue curves) follows the law of the wall [70]; with vegetation, the velocity (green curves) can be approximated as a two-layer distribution [57]. **b**, At the same U_p, vegetation generates additional turbulence and increases the total turbulent kinetic energy. The horizontal dashed lines indicate the upper boundaries of the boundary layers. Compared with the decrease in k_t with increasing z above the boundary layer in the channel without vegetation, the k_t in the vegetated channel is relatively uniform at the upper water column above the boundary layer. The total near-bed k_t has been approximated as the sum of vegetation-generated k_t and the bed-generated k_t [83].

dissipated through a viscous effect, which has a dissipation rate ε classically scaled with $k_t^{3/2}\, l_t^{-1}$ with l_t denoting the turbulence length scale [82]. Assuming that $P_w = \varepsilon$, the scaling relationship becomes $\frac{1}{2}C_D a U_p^3 \sim k_t^{3/2}\, l_t^{-1}$, suggesting that $\frac{\sqrt{k_t}}{U_p} \sim (C_D a l_t)^{1/3}$. Inside an emergent vegetation patch with a vegetation stem diameter much smaller than water depth, the turbulent length scale l_t was shown to be set by the vegetation diameter d_v or the smallest distance between nearest-neighbor stems, whichever is smaller [36,63]. Combining the above scaling relationship and velocity measurements in a flume, Tanino and Nepf [63] proposed the following semi-empirical relationship to predict the spatially-averaged turbulent kinetic energy generated by emergent and rigid cylindrical vegetation arrays with stem diameter smaller than the average surface-to-surface-spacing-between-neighboring cylinders $\langle S_n\rangle_A$:

$$\frac{\sqrt{k_{tv}}}{U_p} = \begin{cases} 1.1\left[C_D\dfrac{\varphi}{(1-\varphi)\pi/2}\right]^{1/3}, & d/\langle S_n\rangle_A < 0.56 \\ 0.88\left[C_D\dfrac{\langle S_n\rangle_A}{d_v}\dfrac{\varphi}{(1-\varphi)\pi/2}\right]^{1/3}, & 0.57 \le d/\langle S_n\rangle_A < 1 \end{cases} \quad (2)$$

For sparse vegetation ($d/\langle S_n\rangle_A < 0.56$ and $\varphi < 10\%$), the vegetation-generated turbulent kinetic energy can be approximated as $k_{t_v} = 1.1^2\left[C_D\frac{\varphi}{\frac{(1-\varphi)\pi}{2}}\right]^{\frac{2}{3}} U_p^2 \approx 0.9C_D^{2/3}\varphi^{2/3}U^2$. The vegetation-generated k_{t_v} is uniformly distributed in the upper water column [36] (Fig. 2b). Equation (2) can predict the vegetation-generated horizontally-averaged k_{t_v} with varying depth over the whole water column, except near the bed where the sediment bed also generates turbulence [42,83]. When the upper water column size is much larger than the size of the boundary layer, the volumetrically-averaged turbulent kinetic energy can also be approximated by equation (2). For natural non-cylindrical plants, such as *Typha latifolia* and *Rotala indica*, the horizontally-averaged k_{t_v} can vary vertically due to the vertical variation of vegetation density, necessitating a modification to equation (2) [84].

Near the sediment bed, the bed generates turbulence and contributes to the total turbulent kinetic energy [42,83]. For sparse cylindrical vegetation with Reynolds number ($Re_P = \frac{\rho U_P d_v}{\mu} = 600-2500$), Yang and Nepf [83] show that the total near-bed turbulent kinetic energy can be approximated as the sum of the vegetation-generated turbulent kinetic energy and the bed-generated turbulent kinetic energy:

$$k_{t\_tot} = C_b U_p^2 + 0.9C_D^{2/3}\varphi^{2/3}U_p^2 \quad (3)$$

where C_b represents the coefficient for bed-generated turbulence and can be approximated from the bed friction coefficient, namely $C_b = 5.3C_f$. Such approximation is based on the observation [84,85] that the bed-generated near-bed turbulence k_t can be approximated as $5.3\tau/\rho$. For vegetation with complex shapes, parameters related to plant morphology also need to be considered [84]. As shown in equations (2) and (3), to evaluate the overall effect of the emergent vegetation on the spatially-averaged turbulent kinetic energy, vegetation impacts on the mean flow velocity U_p and vegetation volume characteristics (φ) need to be considered.

It is worth noting that the above equations are developed for regions within an emergent vegetation patch. At the edge of vegetation patches, the difference in the flow velocity within and outside the vegetation patch can induce shear vortices, generating additional turbulent kinetic energy near the edge of the patches [60,86]. For submerged vegetation, large coherent vortices can be generated at the top of the canopy due to the velocity difference within and above the vegetation; such vortices also generate additional turbulent kinetic energy [81,87–89]. For flexible vegetation, the elasticity of the vegetation can further affect the flow and the generation of turbulent kinetic energy [89,90]. Artificial surrogates, such as plastic blades, have been used to study the effect of flexible vegetation [91,92].

3.3. Impact of vegetation on solute transport

The transport of solutes in water is often predicted by classic advection-dispersion equations for non-reactive solutes. To characterize their transport in vegetated channels, the concentration of solute, C, is defined as the average of its instantaneous concentration over a time interval much longer than the turbulent fluctuation time scale and over a thin volume that spans many vegetation cylinders [63,93]. The concentration C varies with time and space due to advection and dispersion and can be described by the following simplified advection-dispersion equation:

$$\frac{\partial C}{\partial t}+U_p\frac{\partial C}{\partial x}+V_p\frac{\partial C}{\partial y}+W_p\frac{\partial C}{\partial z}=D_x\frac{\partial^2 C}{\partial x^2}+D_y\frac{\partial^2 C}{\partial y^2}+D_z\frac{\partial^2 C}{\partial z^2} \tag{4}$$

where U_p, V_p, and W_p denote the mean flow velocity averaged within a thin volume defined above in the streamwise or longitudinal (x), lateral (y), and vertical (z) directions, respectively; D_x, D_y, and D_z denote the net dispersion coefficients in each direction. The second to fourth terms on the equation's left-hand side represent the advection of the solute by the mean flow in each direction. The terms on the right-hand side of the equation represent the net dispersion of the solute in each direction, which is controlled by molecular diffusion, turbulent diffusion, and mechanical dispersion caused by a spatially-heterogeneous flow field [63,94,95]. If the flow is unidirectional in the streamwise or x-direction, then $V_p = W_p = 0$. Equation (4) can be simplified as:

$$\frac{\partial C}{\partial t}+U_p\frac{\partial C}{\partial x}=D_x\frac{\partial^2 C}{\partial x^2}+D_y\frac{\partial^2 C}{\partial y^2}+D_z\frac{\partial^2 C}{\partial z^2} \tag{5}$$

In a turbulent flow, the molecular diffusion is much smaller than the turbulent diffusion, thus the dispersion coefficients are mainly determined by eddy viscosity. In an open channel without vegetation, the turbulence is predominantly generated by the bed. As a result, the dispersion coefficients scale with the bed friction velocity $u_{b*}=\sqrt{\frac{\tau_b}{\rho}}$, where τ_b represents the mean bed shear stress, defined as the friction force exerted by water at the sediment bed per unit area.

Vegetation has been shown to play an important role in the transport of solutes in natural aquatic ecosystems [93,96] because it can alter advection by controlling the mean surface flow velocity and the dispersion coefficients [38,63]. First, at the same water surface slope s, vegetation slows down U_p and decreases the advection of solutes (see Section 3.1 for impacts of vegetation on mean flow). On the other hand, under the same mean flow velocity U_p, vegetation increases the dispersion of solutes by generating turbulence that increases turbulent diffusion and induces mechanical diffusion by making the flow field spatially heterogeneous [39,93]. As a result of the vegetation-generated turbulence and mechanical dispersion, the effective dispersion coefficients in a vegetated channel scale with vegetation density and stem diameter, instead of the bed friction velocity. The dispersion coefficients in vegetated channels are anisotropic as discussed below.

In the streamwise direction, White and Nepf [97] proposed estimating the dispersion coefficient D_x as the sum of the diffusion coefficient due to vortex tapping D_{x-v} and the coefficient due to stem-wake D_{x-s} at moderate Reynolds number (Re_D on the order of 10−1000). They further show that D_{x-v} can be predicted by vegetation density a, stem diameter d, flow velocity U_p, and the frequency of vortex shedding f_s as [97]:

$$D_{x-v}=\frac{\beta\kappa_v}{St}ad_vU_pd_v \tag{6}$$

where constants β and κ_v are coefficients determined by the stem Reynolds number $Re_P=\frac{\rho U_P d_v}{\mu}$; $St=\frac{f_s d_v}{U_p}$ represents the Strouhal number and describes the effect of the oscillating vortex shredded from the vegetation [78]. The dispersion coefficient due to secondary wake D_{x-s} has been approximated as [38,93,98]:

$$D_{x-s}=\begin{cases}\frac{1}{2}C_D^{3/2}U_pd_v, \varphi<0.1\\ 5ad_vU_pd_v, \varphi>0.1\end{cases} \tag{7}$$

The total longitudinal dispersion coefficient is thus $D_x = D_{x-v}+D_{x-s}$. For real vegetation such as winter and summer *Typha*, flume experiments show that the net longitudinal dispersion coefficient is approximately $D_x\approx 3U_pd_v$ [93]. In contrast, for *Carex*, another vegetation with a different morphology, it is approximated that $D_x\approx 18U_pd_v$, suggesting that the type and heterogeneous morphology of stems also impact the dispersion coefficients [93].

In the lateral direction, the net dispersion coefficient D_y has been estimated as the sum of the turbulent diffusion and mechanical dispersion coefficients [36,63]. For cylindrical vegetation, Nepf [36] suggests that the turbulent diffusion scales with the square root of turbulent kinetic energy k_t times the turbulent length scale l_t. She further suggests that the mechanical dispersion coefficient scales with the vegetation density, flow velocity, and stem size [36]. As a result, the net lateral dispersion coefficient can be estimated as:

$$D_y\sim k_t^{1/2}\,l_t+ad_vU_pd_v \tag{8}$$

Tanino and Nepf [63] built on this scaling relationship and developed another semi-empirical equation for D_y, taking into account the tortuosity of the flow path within the vegetation array. Nepf [31] further suggests that D_y can be empirically approximated as $0.2U_pd_v$ for sparse vegetation ($\varphi<0.1$) and as $U_pd_v\varphi$ for dense vegetation ($\varphi>0.1$). Based on experiments with cylindrical vegetation, these models have been shown to provide reasonable approximations for some natural vegetation, such as summer *Typha* and *Spartina*. Yet, they underestimate other vegetation, such as *Phragmites* and new winter *Typha* [93]. In the vertical direction, Nepf [36,40] suggests that the dispersion coefficient D_z due to turbulence also scales with $k_t^{1/2}\,l_t$, similar to the lateral dispersion coefficient. However, the scaling factors for the vertical and lateral dispersion coefficients are different because the turbulent is not isotropic [36,40]. Lightbody and Nepf [38] further suggest that $D_z=\alpha\sqrt[3]{C_Dad_v}u_pd_v$ with the scaling parameter $\alpha = 0.1$–0.2 for $ad_v<0.1$. Some key parameters and equations from the above studies are listed in Table 2.

To evaluate the overall impact of vegetation on the transport of solutes, the two competing effects, namely the reduction in advection and dispersion due to the slowdown of the flow and increase in dispersion due to vegetation-generated turbulence, need to be considered together. Inside a vegetated channel or vegetation patch away from the edge, flow velocity reduction dominates, leading to observed increases in net deposition [99,100]. In contrast, at the edges of vegetation patches, a reduction in net deposition has been observed [101,102], suggesting enhanced dispersion. This effect is attributed to the additional shear vortices generated at the interface between the vegetated patch and the open channel, further increasing solute dispersion [60,103].

Table 2
A list of some key parameters and equations in several recent studies on the dispersion coefficients inside vegetation canopies.

Dispersion coefficients	Reference	Vegetation characteristics	Reynolds number	Reference
$D_x = D_{x-v} + D_{x-s}$ $D_{x-v} = \frac{\beta \kappa_v}{St} a d_v U_p d_v$ $D_{x-s} = f(a, d_v, U_p, D_m, C_D, \rho, \mu)$	[97]	Random cylinder arrays, $\varphi = 0.01-0.05$	Re_D on the order of 10–1000	[97]
$D_{x-s} = \frac{1}{2} C_D^{3/2} U_p d_v$ $D_z = \alpha \sqrt[3]{C_D a d_v} u_p d_v$; $\alpha = 0.1-0.2$	[38]	Spartina alterniflora, $\varphi = 0.001-0.012$	$Re_D = 2-360$	[38]
$D_{x-s} = 5 a d_v U_p d_v$	[98]	Random cylinder arrays, $\varphi = 0.012-0.038$	$Re_D = 20-580$	[98]
$D_y \sim k_t^{1/2} l_t + a d_v U_p d_v$ $D_z \sim k_t^{1/2} l_t$	[36]	Random cylinder arrays, Spartina alterniflora; $\varphi = 0.006-0.055$	$Re_D = 200-600$	[36]
$\frac{D_y}{U_p d_v} = f(d_v, \varphi, \langle S_n \rangle_A)$	[63]	Random cylinder arrays, $\varphi = 0.010-0.035$;	Reynolds number based on pore size $Re_s > 250$	[63]
$D_y \approx 0.2 U_p d_v$ for $\varphi < 0.1$ and $U_p d_v \varphi$ for $\varphi > 0.1$	[31] (a review)	Cylinder arrays	All Reynolds number	[31] (a review)
$D_x \approx 18 U_p d_v$ and 3 $U_p d_v$ for *Carex* and both *Typha latifolia, respectively*; $D_y \approx U_p d_v$ for *Carex* and winter *Typha*; $D_y \approx 0.2 U_p d_v$ for summer *Typha*	[93]	Regular cylinder arrays; Random real vegetation (*Carex acutiformis*, winter *Typha latifolia*, and summer *Typha latifolia*), $\varphi = 0.005-0.08$	$Re_D = 27-524$	[93]

4. Impacts of vegetation on the transport of particles

Compared with the transport of solutes, the transport of particles, such as sediment, can occur as wash load, suspended load, or bedload [104]. Wash load refers to the transport of ultra-fine particles, such as fine sediment with a size of <0.0625 mm, whose gravitational effect is negligible [105]. Their transport is similar to solutes and is often predicted by the advection-dispersion equation described above [106]. Accordingly, the impact of vegetation on wash load transport is expected to be similar to its impact on solute transport, as discussed in Section 3.3. Suspended load refers to the fine particles in suspension, and bedload refers to coarse particles that move along the bed through rolling, sliding, and hopping [70]. Sediment is the most extensively studied particle, given its crucial role in habitat stability, biogeochemical cycles, and pollutant transport [9–20]. For low-density particles such as plastics, surface transport or transport in the water-air interface also occurs due to the buoyancy effect [107]. This section focuses on equations to predict the sediment transport, including suspended load and bedload transport, and the impacts of vegetation on such transport. The application of these equations to other particles is briefly discussed.

4.1. Impact of vegetation on suspended load transport

4.1.1. Classic equations for suspended sediment transport

Compared with solutes with negligible gravity, the transport of suspended fine sediment is impacted by gravity. An important parameter to characterize suspended load transport is the settling velocity w_s. Settling velocity is the equilibrium velocity when one suspended particle falls through the water column, during which its drag force induced by the settling motion balances its gravitational force. For small non-cohesive spherical particles with diameter $d_s < 0.1$ mm, the flow around the particle is laminar. The particle Reynolds number $Re_{ds} = \frac{\rho w_s d_s}{\mu} < 1$, thus the settling velocity can be predicted by Stokes' law [108,109]:

$$w_s = \frac{(\rho_s - \rho) g d_s^2}{C_1 \mu} \tag{9}$$

where ρ_s is the density of the particle, g is the gravitational acceleration. The coefficient $C_1 = 18$ was derived theoretically based on the balance of the drag force in a laminar flow and the gravitational force [108]. When the particles are non-spherical or have non-smooth surfaces, the coefficient C_1 is usually larger than 18 [110,111]. For particles with different sizes, shapes, and densities, Ferguson and Church [112] proposed the following semi-empirical equation to predict their settling velocity:

$$w_s = \frac{R g d_s^2}{C_1 \nu + (0.75 C_2 R g d_s)^{0.5}} \tag{10}$$

where $R = \frac{\rho_s}{\rho} - 1$ and the kinematic viscosity $\nu = \mu/\rho$. They further suggest that $C_1 \approx 18$ and $C_2 \approx 0.4$ for smooth spheres, $C_1 \approx 24$ and $C_2 \approx 1.2$ for angular natural sediment grains, and $C_1 \approx 18$ and $C_2 \approx 1.0$ for sediment grains with intermediate shapes [112]. Equation (10) only applies to dilute suspension, for which the impacts of particle motion on the fluid flow are neglected. For highly concentrated suspension, the suspended particles can interact with each other, and form flocculates [113,114], which impact the fluid properties (e.g., density and viscosity), the fluid flow field, and the particle transport [115,116].

The transport of suspended sediment is classically called suspended load/sediment transport [70]. An important parameter to quantify such transport is the time-averaged concentration of suspended sediment, C_s, defined as the mass of sediment per unit total volume (including both sediment and water volume) [70]. For fully-developed unidirectional flow at a steady state, i.e., the flow and sediment concentration does not change with time, the sediment concentration is mainly a function of vertical distance from the bed, namely $C_s(z)$. The vertical distribution (in z-direction) of C_s can be predicted by the Rouse profile based on mass and momentum balance [117]. For open channel flow without vegetation, C_s decreases with increasing vertical distance from the sediment bed. At equilibrium, the mass of suspended sediment at any control volume does not change with time; thus, the downward advective flux due to sedimentation, $C_s w_s$, is equal to the upward diffusive flux due to sediment concentration gradient at any location z. The upward diffusive flux is often caused by the turbulent mixing of sediment. It can be approximated as $\varepsilon_z \frac{\partial C_s}{\partial z}$ with ε_z denoting the turbulent diffusion coefficient for suspended sediment. For the total flux to be zero at any vertical location:

$$C_s w_s + \varepsilon_z \frac{\partial C_s}{\partial z} = 0 \tag{11}$$

If ε_z is a constant, the variation of sediment concentration in the

vertical direction is approximately exponential; namely $C_s = C_0 e^{-w_s z/\varepsilon_z}$. For open channel flow with a logarithmic velocity distribution (the law of the wall), the vertical mixing coefficient ε_z is often approximated as a function of the bed shear velocity and the distance from the bed [70]:

$$\varepsilon_z = \beta_s \kappa u_{b*} \frac{z}{h}(h - z) \tag{12}$$

where $\beta_s \approx 1$ denotes the ratio of sediment diffusion coefficient to turbulent diffusion coefficient, $\kappa \approx 0.4$ denotes the von Karman constant, $u_{b*} = \sqrt{\frac{\tau_b}{\rho}}$ denotes the bed shear velocity, and h denotes water depth [70]. The coefficient β_s is equal to one over the more commonly-used Schmidt's number $Sc = \frac{\nu}{D_m}$ where the kinematic viscosity ν represents the momentum diffusivity and D_m represents the molecular diffusion rate of the solutes or ultrafine particles. Discussions about Schmidt's number can be found in several papers [118,119]. By substituting $\varepsilon_z = \beta_s \kappa u_{b*} \frac{z}{h}(h - z)$ into the advection-diffusion equation for suspended sediment transport (equation (11)), an analytical solution often referred to as Rouse profile can be derived:

$$\frac{C_s}{C_a} = \left(\frac{h - z}{z}\frac{a}{h - a}\right)^{Ro = \frac{w_s}{\beta_s \kappa u_{b*}}} \tag{13}$$

where C_a represents the sediment concentration at a reference vertical location $z = a$, and $Ro = \frac{w_s}{\beta_s \kappa u_{b*}}$ denotes the Rouse number [117]. The Rouse number represents the ratio of the settling effect (indicated by w_s) to the dispersion or mixing of the sediment due to the bed-generated turbulence, which is a function of the bed shear velocity u_{b*}. As the Rouse number increases, gravitational sedimentation plays a more dominant role, and as a result, more suspended sediment accumulates near the sediment bed. In contrast, as the Rouse number decreases, the gravitational effect will play a lesser dominant role, and as such the sediment concentration tends to become more uniform across the water column. More detailed discussions about the vertical mixing coefficient ε_z and Rouse profiles can be found in many papers and books [70,120–122]. The suspended sediment transport rate can be estimated as the depth integral of the suspended sediment concentration.

4.1.2. Impacts of vegetation on suspended sediment concentration

Vegetation has been shown to impact suspended sediment transport by altering the mean flow velocity and turbulent kinetic energy, which control the advection and vertical mixing coefficient, respectively [36,58,84,123]. Many field studies show that vegetation can increase fine sediment deposition [100,124]. This can be attributed to the reduction in mean flow velocity, which reduces the overall mean flow velocity and turbulent kinetic energy. However, in some circumstances, under the same mean flow velocity, vegetation has been shown to increase the suspension of sediment [41,58]. Such enhancement can be attributed to the vegetation-generated turbulence, which alters the vertical mixing coefficient and the suspended sediment concentration profile [41,58]. For an open channel with the streamwise velocity following the law of the wall (Fig. 2), the vertical mixing coefficient ε_z scales with the bed friction velocity and follows a parabolic distribution (equation (12)) [70]. In contrast, in channels with vegetation, the velocity is no longer logarithmic [36,57,76], and vegetation generates additional turbulence [36,60]; thus, ε_z is no longer a parabolic function of z, and the Rouse profile (equation (13)) is not applicable [58,84,125]. The following paragraph describes the impact of emergent vegetation on ε_z and recent turbulence-based models to predict the vertical suspended sediment concentration profiles in a vegetated channel.

Flume experiments were conducted to characterize the impact of vegetation-modified flow field and vegetation-generated turbulence on the vertical dispersion of suspended sediment [58,126]. In an emergent cylindrical array, Tseng and Tinoco [58] modified the Rouse profile based on the two-layer velocity distribution proposed by Yang et al. [57] (Fig. 2a). Their model suggests that the sediment concentration follows a two-layer distribution [58] (Fig. 3), similar to the two-layer velocity distribution [57]. Specifically, they propose that the sediment concentration profiles follow a parabolic distribution similar to the velcoity distribution profile in the bottom boundary layer and a uniform concentration layer above this bottom boundary layer [58]:

$$C_s(z) = \begin{cases} C_a\left[\frac{h - z}{z}\frac{a}{h - a}\right]^{Ro_{eff}}, z \le h_b \\ C_a\left[\frac{h - h_b}{h_b}\frac{a}{h - a}\right]^{Ro_{eff}}, z > h_b \end{cases} \tag{14}$$

where h_b denotes the thickness of the effective boundary layer, and $Ro_{eff} = \frac{w_s}{\kappa u_{b*\mathrm{eff}}}$ denotes the effective Rouse number based on the effective bed friction velocity $u_{b*\mathrm{eff}}$. The effective bed friction velocity is a function of vegetation-generated turbulence, incorporating the impacts of vegetation-generated turbulence [58]. The effective boundary layer thickness is a function of bed roughness, flow velocity, and vegetation drag coefficient [58]. For the real plant *Typha latifolia*, Xu and Nepf [126] proposed a diffusivity model. They estimated the dispersion coefficient of suspended sediment based on turbulent kinetic energy and eddy size, similar to the solute dispersion coefficient described in Section 3.3:

$$\varepsilon_z = \alpha \sqrt{k_t} l_t \tag{15}$$

where α is a scale constant on the order of 1 and determined by the vegetation volume fraction and arrangement [84]. For real vegetation whose morphology changes vertically in the z-direction, k_t, l_t, and α all vary with z; semi-empirical equations for these variations for *Typha latifolia* were derived by Xu and Nepf [84]. They further incorporated ε_z into a random displacement model, which simulates the movement of individual particles with particle motion per time step as a function of ε_z, and validated their model prediction using measurements in a flume [126].

4.1.3. Other factors that control suspended sediment transport

In addition to altering the flow field and generating turbulence,

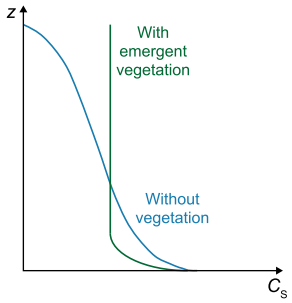

Fig. 3. A schematic diagram showing the impacts of emergent and cylindrical vegetation on the vertical profile of suspended sediment concentration C_s. In an open channel without vegetation, C_s decreases with increasing vertical distance from the sediment bed, following the Rouse profile [117]. In channels with emergent cylindrical and rigid vegetation, C_s in the upper water column becomes uniform due to the mixing of the vegetation-generated turbulence, and a two-layer model was proposed [58].

vegetation surfaces can directly capture and retain fine sediment that contacts the vegetation surfaces [127,128]. Specifically, when suspended sediment moves sufficiently close to the vegetation surfaces, a fraction of the sediment would adhere to the surface, called sediment capture [127,128]. The efficiency of the sediment capture is controlled by the vegetation Reynolds number $Re_D = \frac{\rho U_p d_v}{\mu}$, and the sediment-to-vegetation size ratio $\frac{d_s}{d_v}$, as well as the presence of biofilms [127,128]. Furthermore, vegetation that is not completely vertical can increase the settling of suspended sediment by providing extra (horizontal) surfaces for the sediment to settle [129]. The deposition on vegetation surface is expected to be more significant on tilted and flat vegetation than on vertical and cylindrical vegetation [129].

In addition to sediment, vegetation impacts the suspended transport of many other particles, such as particulate organic matter [130], microplastics [131], contaminant-bound particles [132], and plant seeds [133]. Compared with sediment (e.g., quartz sand), which is often denser than water and settles due to gravity, these particles can have a range of density. For high-density particles, the transport equations developed for sediment have been adapted to predict their transport [107]. As a result, the impacts of vegetation on suspended sediment transport described above should also apply to these particles. For low-density particles, such as buoyant microplastics [107,134], transport along the air-water interface, referred to as surface transport, can be the dominant mode of transport [107]. Vegetation can regulate the surface transport of these particles by altering the flow field near the air-water interface, which controls their advection and dispersion in the wake zone [133]. In addition, vegetation can directly capture the particles that come into contact with the surface [135], similar to the capture of suspended sediment discussed above [127,128]. Furthermore, due to surface tension, the water surface around the vegetation stems can rise and form a meniscus surface; such an effect has been shown to trap floating particles close to the vegetation [133,136]. The transport of these non-sediment particles is also impacted by many other factors, such as particle shape, interactions with biofilms, and degradation [107].

4.2. Impacts of vegetation on bedload transport

4.2.1. Classic equations for bedload transport

Critical shear stress and bedload transport are the most commonly used parameters to characterize bedload transport rate. The critical shear stress, τ_{crit}, refers to the mean bed shear stress above which sediment starts to move. Above the critical shear stress, coarse sediment grains roll, slide, or hop within a thin bedload layer, which is about several grain sizes above the sediment bed [70,137]. The volume (or mass depending on the definition) of the sediment moving as bedload per unit channel width per time is referred to as bedload transport rate Q_s. τ_{crit} is classically predicted from the flow condition and sediment properties [138], and Q_s is often expressed as a function of the flow condition, particularly the mean bed shear stress τ_b [70]. This section reviews classic equations to predict the τ_{crit} and Q_s for abiotic non-cohesive sediment.

The critical shear stress τ_{crit} and its equivalent, the critical shear velocity $u_{crit*} = \sqrt{\frac{\tau_{crit}}{\rho}}$, are often predicted from the classic Shields or modified Shields Diagram [138]. In the classic Shields diagram [138], the non-dimensional critical shear stress $\tau_{crit*} = \frac{\tau_{crit}}{(\rho_s-\rho)gd_s}$ is plotted semi-empirically against the grain shear Reynolds number based on the bed shear velocity, $Re_* = \frac{u_{crit*}d_s}{\nu}$. Note that the subscript "*" in τ_{crit*} means non-dimensional parameter, while the same subscript in u_* and Re_* means the velocity is the friction velocity instead of the flow velocity. As τ_{crit} and its equivalent u_{crit*} are involved in both axes of the Shields diagram, and an iteration is needed to calculate τ_{crit} and u_{crit*} from the semi-empirical Shields diagram based on the fluid properties (ρ, ν) and the sediment properties (ρ_s, d_s), as well as the gravitational acceleration constant (g). To reduce the iterative process, several explicit formulas, or modifications of the original Shields diagram, have been proposed [139,140]. For example, some studies [141,142] modified Shields Diagram and plotted τ_{crit*} as a semi-empirical function of the grain Reynolds number based on the grain size, $Re_g = \frac{\sqrt{gsd_s}d_s}{\nu}$. For quartz sand, a direct empirical relationship between the dimensional critical shear stress τ_{crit} and sediment size d_s has also been proposed [143,144]. In addition to sediment size, the impacts of many other factors on τ_{crit} have also been studied, including the nonuniform distribution of sediment grain sizes [145–147], channel-bed slope [148,149], sediment arrangement or compactness [150,151], sediment cohesiveness [14], and the history of the flow [152].

When the mean bed shear stress τ_b is above τ_{crit}, the movement of the sediment in the bedload layer is often characterized by the sediment transport rate Q_s [70]. Many classic bedload transport equations predict Q_s based on the mean bed shear stress τ_b, such as the DuBoys' equation [153], the Bagnold equation [154], the Meyer-Peter Müller's equation [155,156], and the Einstein-Brown equation [157,158]. Most of these are semi-empirical equations based on laboratory measurements in an open channel without obstacles, and they often have uncertainties over one order of magnitude [159], largely due to the intrinsic stochastic nature of turbulence and bedload transport. One of the most widely used equations is the Meyer-Peter Müller's (MPM) equation [155,156], developed especially for gravel beds. The MPM equation [155,156] suggests that nondimensional bedload transport rate $Q_* = \frac{Q_s}{\sqrt{\left(\frac{\rho_s}{\rho}-1\right)gd_s^3}}$ is proportional to the excess nondimensional shear stress raised to the power of 1.5, specifically $Q_* = \alpha(\tau_* - \tau_{crit*})^{\frac{3}{2}}$ with $\tau_* = \frac{\tau_b}{(\rho_s-\rho)gd_s}$ and the constant parameter α is about 5 [160]. The non-dimensional critical shear stress τ_{crit*} is often approximated as 0.047, despite the large range of value predicted by the Shields diagram [138]. Some other classic bedload equations do not incorporate τ_{crit*} and predict Q_* as a function of τ_* using other types of equations [157,158]. For example, the Einstein-Brown equation [157,158] suggests that $Q_* = 2.15e^{-0.391/\tau_*}$, $40\tau_*^3$, and $15\tau_*^{1.5}$ when $\tau_* < 0.18$, $0.18 < \tau_* < 0.52$, and $0.52 < \tau_*$, respectively. In recent decades, more sophisticated stochastic equations have been proposed to predict Q_s based on parameters that describe particle movement, such as average particle velocity, hop statistics, and activity [161–165]. For cohesive sediment, Q_s is also impacted by many other parameters [14,69,166], such as the percentage of clay, the types of clay, the plasticity of the sediment, the organic content of the sediment, and the chemistry of the pore water. More discussions about different equations to predict the bedload transport rate of abiotic sediment can be found in many review papers and books [70,166–169]. This section focuses on the transport of non-cohesive sediment.

4.2.2. Impact of vegetation on bedload transport

Vegetation has been shown to impact bedload transport, including the critical bed shear stress τ_{crit} and bedload transport rate Q_s, by altering the mean surface flow velocity and the turbulent kinetic energy [41,42,44,59,83,170,171]. Flume experiments and field investigations show that emergent vegetation can reduce τ_{crit} several times [83,172,173]. At the same water surface slope, vegetation has been shown to reduce bedload transport rate, and this

can be attributed to the vegetation-induced decreases in the mean flow velocity and the mean bed shear stress [170]. In contrast, at the same mean flow velocity and mean bed shear stress, vegetation has been shown to increase bedload transport rate by several orders of magnitude [42,44,59]. The overall effect of vegetation on bedload transport results from these two competing effects: the slowdown of the mean flow velocity and the generation of turbulence by vegetation. This section discusses theoretical equations to predict the τ_{crit} and Q_s in channels with emergent vegetation.

For open channel flows without vegetation, τ_{crit} is a function of the sediment characteristics. It should remain a constant for the same sediment bed, according to the original and modified Shields diagrams [138,141,142]. Flume experiments with emergent vegetation show that τ_{crit} decreased by up to four folds with increasing vegetation volume fraction [83,172] due to the vegetation-generated turbulence [56,83]. Compared with the constant τ_{crit} for the non-vegetated channel flow, Yang et al. [83] found that the critical near-bed turbulent kinetic energy when the bedload started to occur, $k_{t\,crit}$, was the same for non-vegetated channels and vegetated channels with different vegetation volume fraction φ. For the same sediment, $k_{t\,crit}$ for the non-vegetated channel is equal to $C_b U^2_{crit\_o}$ with U_{crit_o} denoting the critical flow velocity to move the sediment (see Section 3.2 for details); and $k_{t\,crit}$ for vegetated channel with volume fraction φ is equal to $C_b U^2_{crit\_\varphi} + 0.9 C_D^{2/3} \varphi^{2/3} U^2_{crit\_\varphi}$ with U_{crit_φ} denoting the critical flow velocity to move the sediment in the vegetated channel (equation (3), Section 3.2). By equating the above two $k_{t\,crit}$, Yang et al. [83] derived the following equation to predict the critical mean flow velocity for the sediment to move in channels with emergent vegetation of volume fraction φ:

$$\frac{U_{crit\_\varphi}}{U_{crit\_o}} = \frac{1}{\sqrt{1 + C\varphi^{2/3}}} \tag{16}$$

where $C = 0.9 C_D^{2/3}/C_b$. The bed and vegetation drag coefficients C_b and C_D can be estimated from existing empirical equations [39,68,70]. Following the turbulence-based model, Cheng et al. [174] incorporated the turbulence effect into the drag force term and proposed a theoretical model based on force balance; their model suggests that the critical Froude number $Fr_{crit} = U_{crit\_\varphi}/\sqrt{(\frac{\rho_s}{\rho} - 1) g d_s}$ based on vegetation volume fraction and two fitted constants. Once U_{crit_φ} was estimated from the above models, the critical bed shear stress to move the sediment can be estimated from U_{crit_φ} and vegetation characteristics [57,80].

In addition to the critical condition for bedload transport, vegetation is shown to modify the bedload transport rate by up to three orders of magnitude [42,44,56,59]. As discussed in Section 4.2.1, for open channels without vegetation, Q_s is a function of mean bed shear stress τ_b, namely $Q_s = f(\tau_b)$, according to classic bedload transport equations [153–158]. However, under the same τ_b, the Q_s in vegetated channels increases with increasing vegetation volume fraction φ by up to three orders of magnitude; thus, the τ-based bedload equations do not apply to vegetated channels [42,44,59]. The increase in Q_s with increasing φ at the same τ_b has been attributed to the vegetation-generated turbulence [42,59], which generates a lift force on the sediment and makes it easier to move [42]. In contrast to the order-of-magnitude difference in Q_s between non-vegetated and vegetated channels under the same τ_b, flume experiments by Yang et al. [42] show that at the same total near-bed turbulent kinetic energy k_{t_tot}, the measured Q_s is roughly the same for both non-vegetated and vegetated channels, suggesting that k_{t_tot} is a better predictor of Q_s than τ for vegetated channels. They further show that classic τ-based bedload transport equations can be converted to k_t-based equations, and the converted equations apply to both non-vegetated and vegetated channels [44]. Specifically, for the non-vegetated channels, the bed generated near-bed turbulence k_t can be approximated as $\frac{5.3\tau}{\rho}$ [85], as a result $Q_s = f(\tau_b)$ can be written as $Q_s = g(k_t)$. The converted k_t-based models provide good estimation of Q_s measured in laboratory flumes with emergent vegetation with various diameters and arrangements [42,44,56]. Building on the k_t-based model, Wu et al. [175] incorporated the vegetation-generated k_t into a new hydrodynamic parameter, and a bedload transport model was proposed based on this parameter.

While at the same τ_b, vegetation-generated turbulence increases bedload transport, and vegetation also reduces mean surface flow velocity, which reduces bedload transport. The overall effect of vegetation on bedload transport is the net result of these two competing effects. At the same water surface slope s, for a typical marsh with volume fraction $\varphi = 0.001–0.1$, vegetation has an overall tendency to reduce bedload transport (Fig. 4), due to its reduction in U_p. As equation 1-b suggests, at the same water surface slope, U_p decreases with increasing φ (Fig. 4a). As φ increases and U_p decreases, the bed shear stress τ_b decreases because it scales with U_p^2 when Reynolds number $Re_D > \frac{4}{C_f}$ (equation (14) in Ref. [57]), as shown in Fig. 4b. Similarly, as φ increases, the total turbulent kinetic energy k_t decreases, scaling with U_p^2 as suggested as indicated by equations (2) and (3) (Fig. 4b). However, the vegetation-generated turbulence cause k_t to increase with increasing φ (equation (3) and (4)). As a result, the decrease in k_t with increasing φ is slower than the decrease in τ_b (Fig. 4b). Consequently, the classical τ_b-based bedload transport models, which disregard the vegetation-generated turbulence, may underestimate the bedload transport rate by several orders of magnitude [42,44,59], (Fig. 4d). Similarly, the critical shear stress τ_{crit} predicted by the classic Shields diagram [83,172] is ineffective for vegetated channels because they do not consider the vegetation-generated turbulence. For the same sediment bed, τ_{crit} inside the vegetated channel can

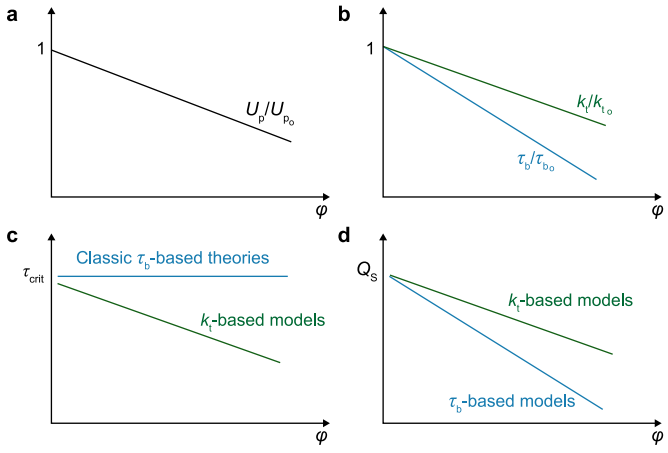

Fig. 4. A schematic diagram showing the impacts of emergent vegetation on the surface flow and bedload transport under the same water surface or energy slope within a vegetation patch. The subscript "o" denotes the value for cases without vegetation, or $\varphi = 0$. **a**, At the same water surface slope, U_p decreases with increasing φ. **b**, Due to the vegetation-generated additional turbulence, with increasing vegetation volume fraction φ, the turbulent kinetic energy k_t decreases much slower than the bed shear stress τ_b. **c**, The classic τ_b-based models overestimate the critical shear stress τ_{crit}. **d**, The classic τ_b-based models underestimate the bedload transport rate Q_s. Note that the lines in the figure show the general tendency instead of the actual relationship, which is not linear.

be several times smaller than the value inside a non-vegetated channel (Fig. 4c). This tendency to reduce bedload transport at the same water surface slope applies to regions within an emergent vegetation patch. However, in other regions, such as near the edge of the vegetation patch, the bedload transport may be higher than in non-vegetated regions due to the shear vortices generated at the edge of vegetation patches [60], further enhancing bedload transport.

4.2.3. The transport of other particles and other bedload transport models

Non-sediment particles, such as many non-buoyant plastics, have been found in the bedload transport layer [176,177]. Many studies proposed using classic bedload transport equations, such as modified Shield diagrams, to predict the transport of these particles [178,179]. Such predictions tend to have a larger uncertainty than sediment due to the various shapes and densities of these particles [175]. In addition, some particles would break and form smaller pieces due to collision with sediment grains during bedload transport [107]; the resultant changes in particle sizes could introduce more uncertainties in bedload transport predictions. Despite the uncertainties in predicting bedload transport of these particles, the impacts of vegetation on bedload transport, resulting from turbulence generation and mean flow deceleration, are expected to also apply to these non-sediment particles.

In addition to the turbulence-based sediment transport models, modifications of classic τ-based models have been proposed to predict sediment transport in vegetated channels [180,181]. These modified τ-based models also show good agreement with experimental data, likely due to the implicit incorporation of turbulent effects in their parameters. For example, Lu et al. proposed a new formula for bed shear stress that incorporates the effect of vegetation-generated turbulence [181]. Some other studies estimate bed shear stress by subtracting the vegetation drag from the total stress [170,182], which may implicitly incorporate the vegetation-turbulence effect in the vegetation drag term.

5. Impact of vegetation on hyporheic exchange

Besides altering the surface flow, vegetation can impact the fate and transport of solutes and particles by altering hyporheic exchange, which involves the exchange of surface and subsurface water and associated chemicals [33,46–48]. Hyporheic exchange occurs when surface water infiltrates into the sediment bed and subsequently returns to the surface water due to a spatial pressure head gradient at the sediment-water interface [7,183]. In addition, it can arise from dispersion, especially turbulent dispersion, at the sediment-water interface [184–186]. Emergent vegetation can impact hyporheic exchange through various mechanisms. First, as vegetation decelerates flow around individual dowels, the flow and pressure head at the sediment-water-interface become heterogeneous inside the vegetation patch [57,76]. In addition, the slowdown of the flow at the upstream side of each vegetation stem can induce a vertical pressure gradient that drives surface water into the sediment bed at the upstream side of the stem and then back to the surface water at the downstream side of the stem [49] (Fig. 5) These stem-scale heterogeneity and vertical flux contribute to the exchange between surface and subsurface water or hyporheic exchange [48,187]. Second, at the same mean flow velocity, vegetation generates additional turbulence (see Section 3.2 for details), which can increase dispersion at the sediment-water interface and thus increase hyporheic exchange [33]. Third, at the same mean surface flow velocity, the water surface slope in a vegetated channel is larger than that in a non-vegetated channel due to the vegetation drag, as shown in equation (1). As a result, the streamwise pressure

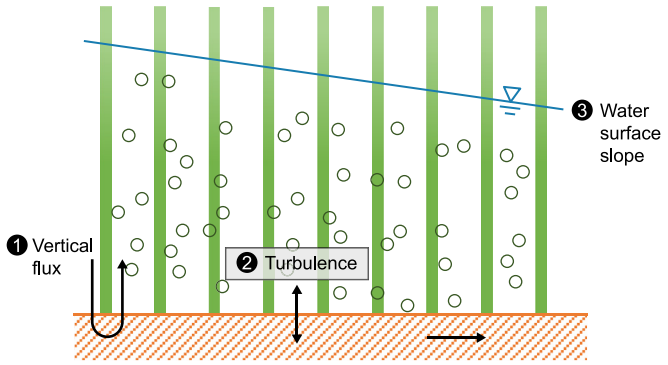

Fig. 5. A schematic diagram showing the major mechanisms by which vegetation impact hyporheic exchange. (1) Vegetation generates stem-scale heterogeneity and vertical flux. (2) Vegetation generates additional turbulence, increasing the dispersion across the sediment-water interface. (3) At the same spatially averaged velocity, the water surface slope is much larger in vegetated channels than in non-vegetated channels. The streamwise pressure gradient can induce a streamwise flow within the sediment bed, increasing hyporheic exchange.

gradient at the sediment-water interface is greater in the vegetated channel than non-vegetated channels. Such vegetation patch-scale pressure gradient is likely to further enhance hyporheic exchange, necessitating further investigation. Recent research shows that the hyporheic exchange velocity between surface and subsurface water scales with the turbulent kinetic energy [33]. Similarly, another recent study suggests that the diffusion coefficient of gas transfer across the sediment-water interface is a function of the near-bed vegetation-generated turbulent kinetic energy [188]. The dependence of the near-bed hyporheic change on the turbulent kinetic energy is likely due to its reflection of both stem-scale heterogeneity and vegetation-generated turbulence.

In addition, similar to the surface flow, hyporheic exchange can be generated near the edge of vegetation patches due to the velocity difference between the vegetated and unvegetated regions and the shear vortices generated at the edge [173,189,190]. The velocity difference between the vegetated and non-vegetated regions can induce a spatial gradient of pressure head, potentially generating hyporheic exchange. In addition, the elevated near-bed turbulence due to the shear vortices can further enhance the dispersion at the sediment-water interface near the edge of the vegetation patch. The impact of vegetation patches on hyporheic exchange is still under-investigated. Similarly, for submerged vegetation, the shear vortices generated at the interface between the vegetation and the upper water layer are likely to generate additional spatial gradients in pressure head and turbulence at the sediment-water interface, further facilitating hyporheic exchange. The impacts of vegetation submergence and other characteristics, such as flexibility, on hyporheic exchange remain to be investigated.

6. Other vegetation-related factors and future research directions

In addition to emergent and rigid vegetation discussed above, the flow and transport in aquatic ecosystems with vegetation are impacted by many other vegetation-related factors, including vegetation morphology, submergence, patchiness, flexibility, root structures and exudates, biofilms, fine sediment accumulation, etc. First, natural vegetation can have different morphology [84,191,192], leading to a vertical variation in the vegetation frontal area. As a result, the velocity may vary vertically and no longer follow the uniform distribution across the water depth (Fig. 3).

Second, if the vegetation is submerged, shear vortices are generated near the interface between the vegetation and the upper water layer [31,88]. These vortices can penetrate the vegetation layer and play a critical role in mass transport [45,193–195]. Third, if the vegetation forms patches, the velocity inside and outside will be different, generating shear vortices at the edges of the patches [78–80]. The difference in flow velocity between vegetated and non-vegetated regions can alter dispersion and solute transport [196]. The vortices at the edge of the patch can reduce sediment deposition [60,103] and increase scours near the edge of the patch [173,189,190]. Fourth, flexible vegetation will reshape with flow, potentially influencing flow dynamics and transport processes [89–91]. The wave movement (monami) of flexible vegetation has been shown to affect the near-bed turbulent kinetic energy [31] and bedload transport [197,198]. Fifth, vegetation roots can hold the soil and produce root exudates, enhancing sediment stability [199,200]. Furthermore, vegetation alters the bacterial community and the formation of biofilms [201,202], affecting the fate and transport of nutrients and sediment [203,204] and hyporheic exchange [205]. Moreover, vegetation can promote the accumulation of fine cohesive sediment [206], leading to changes in chemical transport due to adsorption and desorption [207,208], altering sediment transport rate by several orders of magnitude [14,166], and modifying hyporheic exchange [209].

To further understand how vegetation affects the fate and transport of fluid and chemicals in aquatic environments, I recommend the following research directions.

(1) The role of spatial heterogeneity in vegetation size, morphology, flexibility, and patchiness on the flow and transport of solutes and particles.
(2) The role of vegetation on the accumulation of fine cohesive sediment and its impact on sediment transport and hyporheic exchange.
(3) The role of vegetation on the accumulation of organic matter and biofilms in sediment and their impacts on sediment transport and hyporheic exchange.
(4) The mutual interactions between vegetation, flow, and sediment, namely how flow and sediment accumulation impact vegetation growth, which in turn impacts flow and sediment transport.
(5) Incorporation of the laboratory-derived mechanisms in the numerical simulation of transport processes at the field scale and comparison of the results with field observations.

7. Conclusions

In-channel vegetation plays a critical role in the flow and mass transport in aquatic environments. This review provides an overview of the impact of emergent and rigid cylindrical vegetation on mean surface flow velocity, turbulent kinetic energy, advection and diffusion of solutes, suspended load, bedload transport, and hyporheic exchange. The review discusses predictive equations based on laboratory flume experiments. Inside an emergent vegetation patch, the mean flow velocity, turbulent kinetic energy, and the dispersion coefficients of solutes can be predicted by the vegetation characteristics, such as vegetation drag coefficient, density, and stem diameter. The velocity and suspended sediment concentration profiles deviate from logarithmic and Rouse distributions, respectively. Instead, both profiles can be approximated using two-layer distribution models. Classic bedload transport models relying on bed shear stress are ineffective due to vegetation-generated turbulence. Turbulence-based models have been proposed and successfully predict the critical velocity and bedload transport rate. The exchange velocity between surface and subsurface water scales with the total turbulent kinetic energy inside the vegetation patch.

The two competing effects of vegetation on the flow and mass transport are discussed. On the one hand, vegetation slows down the mean flow velocity under the same water surface slope, reducing advection and dispersion of solutes, suspended load transport, bedload transport, and hyporheic exchange. On the other hand, at the same mean flow velocity, vegetation generates additional turbulence, which increases the dispersion of solutes, suspended load transport, bedload transport, and hyporheic exchange. At the same water surface slope, the reduction in the mean flow velocity by emergent vegetation plays a more dominant role. As a result, the transport of solutes, suspended load, bedload, and hyporheic exchange are often reduced inside an emergent vegetation patch (away from the edge of the patch). While emergent vegetation reduces mass transport at the same water surface slope, classic transport models, such as the mean shear stress-based bedload transport models, can underestimate mass transport rate by several orders of magnitude because they do not account for the vegetation-generated turbulence. This review proposes and discusses turbulence-based models and modifications to address this phenomenon.

In addition to emergent and rigid vegetation, various other vegetation-related factors influence flow dynamics and mass transport. These factors include vegetation morphology, submergence, patchiness, flexibility, organic matter, biofilms, and fine sediment accumulation. Future research directions are suggested further to understand flow and mass transport in regions with vegetation.

CRediT authorship contribution statement

Judy Q. Yang: Conceptualization, Funding Acquisition, Investigation, Resources, Writing - Original Draft, Writing - Review & Editing.

Declaration of competing interest

The authors declare that they have no known competing financial interests or personal relationships that could have appeared to influence the work reported in this paper.

Acknowledgements

The author was supported by the United States National Science Foundation through grants EAR 2209591, 2150796, and 2236497.

Appendix A. Supplementary data

Supplementary data to this article can be found online at https://doi.org/10.1016/j.ese.2024.100429.

References

[1] J.D. Allan, Stream Ecology: Structure and Function of Running Waters, Springer Nature, 2020.
[2] R.S. Stelzer, J. Heffernan, G.E. Likens, The influence of dissolved nutrients and particulate organic matter quality on microbial respiration and biomass in a forest stream, Freshw. Biol. 48 (11) (2003) 1925–1937, https://doi.org/10.1046/j.1365-2427.2003.01141.x.
[3] W.A. Wurtsbaugh, Nutrients, eutrophication and harmful algal blooms along the freshwater to marine continuum, Wiley interdisciplinary reviews. Water 7 (4) (2020) e1453, https://doi.org/10.1002/wat2.1453.
[4] O.A.H. Jones, N. Voulvoulis, J.N. Lester, Human pharmaceuticals in the aquatic environment a review, Environmental technology 22 (12) (2001) 1383–1394, https://doi.org/10.1080/09593330.2001.11090873.
[5] M. Dunier, A.K. Siwicki, Effects of pesticides and other organic pollutants in the aquatic environment on immunity of fish: a review, Fish Shellfish

Immunol. 3 (6) (1993) 423–438, https://doi.org/10.1006/fsim.1993.1042.
[6] J.L. Schnoor, Environmental Modeling : Fate and Transport of Pollutants in Water, Air, and Soil, 1996.
[7] F. Boano, J.W. Harvey, A. Marion, A.I. Packman, R. Revelli, L. Ridolfi, A. Wörman, Hyporheic flow and transport processes: mechanisms, models, and biogeochemical implications, Rev. Geophys. 52 (4) (1985) 603–679, https://doi.org/10.1002/2012RG000417, 2014.
[8] J.L. Florsheim, J.F. Mount, A. Chin, Bank erosion as a Desirable Attribute of rivers, Bioscience 58 (6) (2008) 519–529, https://doi.org/10.1641/B580608.
[9] J. Pitlick, P. Wilcock, Relations between streamflow, sediment transport, and aquatic habitat in regulated rivers, Geomorphic processes and riverine habitat 4 (2001) 185–198.
[10] M.F. Stokes, D. Kim, S.F. Gallen, E. Benavides, B.P. Keck, J. Wood, S.L. Goldberg, I.J. Larsen, J.M. Mollish, J.W. Simmons, et al., Erosion of heterogeneous rock drives diversification of Appalachian fishes, Science (American Association for the Advancement of Science) 380 (6647) (2023) 855–859, https://doi.org/10.1126/science.add9791.
[11] R.J. Davies-Colley, D.G. Smith, Turbidity SUSPENI)ED sediment, and water CLARITY: a review, J. Am. Water Resour. Assoc. 37 (5) (2001) 1085–1101, https://doi.org/10.1111/j.1752-1688.2001.tb03624.x.
[12] D.H. Wilber, D.G. Clarke, Biological effects of suspended sediments: a review of suspended sediment impacts on fish and shellfish with relation to Dredging Activities in estuaries, N. Am. J. Fish. Manag. 21 (4) (2001) 855–875, https://doi.org/10.1577/1548-8675(2001)021<0855:BEOSSA>2.0.CO2.
[13] W.E. Robinson, W.E. Wehling, M.P. Morse, The effect of suspended clay on feeding and digestive efficiency of the surf clam, Spisula solidissima (Dillwyn), Journal of experimental marine biology and ecology 74 (1) (1984) 1–12, https://doi.org/10.1016/0022-0981(84)90034-0.
[14] R.C. Grabowski, I.G. Droppo, G. Wharton, Erodibility of cohesive sediment; the importance of sediment properties, Earth Sci. Rev. 105 (3–4) (2011) 101–120, https://doi.org/10.1016/j.earscirev.2011.01.008.
[15] J.A. Arruda, G.R. Marzolf, R.T. Faulk, The role of suspended sediments in the Nutrition of Zooplankton in Turbid Reservoirs, Ecology (Durham) 64 (5) (1983) 1225–1235, https://doi.org/10.2307/1937831.
[16] M. Zhang, R.A. Francis, M.A. Chadwick, Nutrient dynamics at the sediment-water interface: influence of Wastewater Effluents, Environmental processes 8 (4) (2021) 1337–1357, https://doi.org/10.1007/s40710-021-00540-0.
[17] L.T. Thorne, G. Nickless, The relation between heavy metals and particle size fractions within the Severn Estuary (U.K.) inter-tidal sediments, Science of the total environment 19 (3) (1981) 207–213, https://doi.org/10.1016/0048-9697(81)90017-6.
[18] C. Zhang, Z.-g. Yu, G.-m. Zeng, M. Jiang, Z.-z. Yang, F. Cui, M.-y. Zhu, L.-q. Shen, L. Hu, Effects of sediment geochemical properties on heavy metal bioavailability, Environ. Int. 73 (2014) 270–281, https://doi.org/10.1016/j.envint.2014.08.010.
[19] A.T. Kan, G. Fu, M.B. Tomson, Adsorption/desorption Hysteresis in organic pollutant and soil/sediment interaction, Environmental science & technology 28 (5) (1994) 859–867, https://doi.org/10.1021/es00054a017.
[20] J.P. Gao, J. Maguhn, P. Spitzauer, A. Kettrup, Sorption of pesticides in the sediment of the Teufelsweiher Pond (Southern Germany)I, Equilibrium assessments, effect of organic carbon content and pH, Water Res. 32 (5) (1998) 1662–1672, https://doi.org/10.1016/S0043-1354(97)00377-1.
[21] S.K. Malham, P. Rajko-Nenow, E. Howlett, K.E. Tuson, T.L. Perkins, D.W. Pallett, H. Wang, C.F. Jago, D.L. Jones, J.E. McDonald, The interaction of human microbial pathogens, particulate material and nutrients in estuarine environments and their impacts on recreational and shellfish waters, Environmental science–processes & impacts 16 (9) (2014) 2145–2155, https://doi.org/10.1039/c4em00031e.
[22] G.D. O'Mullan, A.R. Juhl, R. Reichert, E. Schneider, N. Martinez, Patterns of sediment-associated fecal indicator bacteria in an urban estuary: Benthic-pelagic coupling and implications for shoreline water quality, The Science of the total environment 656 (2019) 1168–1177, https://doi.org/10.1016/j.scitotenv.2018.11.405.
[23] A. Turner, G.E. Millward, Suspended particles: their role in estuarine biogeochemical cycles, Estuar. Coast Shelf Sci. 55 (6) (2002) 857–883, https://doi.org/10.1006/ecss.2002.1033.
[24] R.C. Jamieson, D.M. Joy, H. Lee, R. Kostaschuk, R.J. Gordon, Resuspension of sediment-associated Escherichia coli in a natural stream, J. Environ. Qual. 34 (2) (2005) 581–589, https://doi.org/10.2134/jeq2005.0581.
[25] D.H. Schoellhamer, T.E. Mumley, J.E. Leatherbarrow, Suspended sediment and sediment-associated contaminants in San Francisco Bay, Environ. Res. 105 (1) (2007) 119–131, https://doi.org/10.1016/j.envres.2007.02.002.
[26] P. McLaren, D.I. Little, The effects of sediment transport on contaminant dispersal an example from Milford Haven, Mar. Pollut. Bull. 18 (11) (1987) 586–594, https://doi.org/10.1016/0025-326X(87)90278-5.
[27] W. He, M. Chen, M.A. Schlautman, J. Hur, Dynamic exchanges between DOM and POM pools in coastal and inland aquatic ecosystems: a review, The Science of the total environment 551–552 (2016) 415–428, https://doi.org/10.1016/j.scitotenv.2016.02.031.
[28] S. Xu, J. Ma, R. Ji, K. Pan, A.-J. Miao, Microplastics in aquatic environments: occurrence, accumulation, and biological effects, The Science of the total environment 703 (2020) 134699, https://doi.org/10.1016/j.scitotenv.2019.134699.
[29] M. Repasch, J.S. Scheingross, N. Hovius, A. Vieth-Hillebrand, C.W. Mueller, C. Höschen, R.N. Szupiany, D. Sachse, River organic carbon Fluxes Modulated by hydrodynamic Sorting of particulate organic matter, Geophys. Res. Lett. 49 (3) (2022), https://doi.org/10.1029/2021GL096343 n/a.
[30] S. Zhang, W. Wang, P. Yan, J. Wang, S. Yan, X. Liu, M. Aurangzeib, Microplastic migration and distribution in the terrestrial and aquatic environments: a threat to biotic safety, J. Environ. Manag. 333 (2023), https://doi.org/10.1016/j.jenvman.2023.117412, 117412-117412.
[31] H.M. Nepf, Flow and transport in regions with aquatic vegetation, Annu. Rev. Fluid Mech. 44 (1) (2012) 123–142, https://doi.org/10.1146/annurev-fluid-120710-101048.
[32] H.M. Nepf, Hydrodynamics of vegetated channels, J. Hydraul. Res. 50 (3) (2012) 262–279, https://doi.org/10.1080/00221686.2012.696559.
[33] S. Huang, J.Q. Yang, Impacts of emergent vegetation on hyporheic exchange, Geophys. Res. Lett. 49 (13) (2022) n/a, https://doi.org/10.1029/2022GL099095.
[34] C. Wang, S.-s. Zheng, P.-f. Wang, J. Hou, Interactions between vegetation, water flow and sediment transport : A review, Journal of hydrodynamics. Series B 27 (1) (2015) 24–37, https://doi.org/10.1016/S1001-6058(15)60453-X.
[35] A. Vargas-Luna, A. Crosato, W.S.J. Uijttewaal, Effects of vegetation on flow and sediment transport; comparative analyses and validation of predicting models, Earth Surf. Process. Landforms 40 (2) (2015) 157–176, https://doi.org/10.1002/esp.3633.
[36] H.M. Nepf, Drag, turbulence, and diffusion in flow through emergent vegetation, Water Resour. Res. 35 (2) (1999) 479–489, https://doi.org/10.1029/1998WR900069.
[37] V. Etminan, R.J. Lowe, M. Ghisalberti, A new model for predicting the drag exerted by vegetation canopies, Water Resour. Res. 53 (4) (2017) 3179–3196, https://doi.org/10.1002/2016WR020090.
[38] F.L. Anne, H.M. Nepf, Prediction of velocity profiles and longitudinal dispersion in emergent salt marsh vegetation, Limnol. Oceanogr. 51 (1) (2006) 218–228, https://doi.org/10.4319/lo.2006.51.1.0218.
[39] Y. Tanino, H.M. Nepf, Laboratory investigation of mean drag in a random array of rigid, emergent cylinders, J. Hydraul. Eng. 134 (1) (2008) 34–41, https://doi.org/10.1061/(ASCE)0733-9429(2008)134:1(34).
[40] H.M. Nepf, J.A. Sullivan, R.A. Zavistoski, A model for diffusion within emergent vegetation, Limnol. Oceanogr. 42 (8) (1997) 1735–1745, https://doi.org/10.4319/lo.1997.42.8.1735.
[41] R.O. Tinoco, G. Coco, Turbulence as the main driver of resuspension in oscillatory flow through vegetation, Jl of geophysical research. Earth surface 123 (5) (2018) 891–904, https://doi.org/10.1002/2017JF004504.
[42] J.Q. Yang, H.M. Nepf, A turbulence-based bed-load transport model for bare and vegetated channels, 19, Geophys. Res. Lett. 45 (10) (2018), https://doi.org/10.1029/2018GL079319, 428-410,436.
[43] A.C. Ortiz, A. Ashton, H. Nepf, Mean and turbulent velocity fields near rigid and flexible plants and the implications for deposition, Jl of geophysical research. Earth surface 118 (4) (2013) 2585–2599, https://doi.org/10.1002/2013JF002858.
[44] J.Q. Yang, H.M. Nepf, Impact of vegetation on bed load transport rate and Bedform characteristics, Water Resour. Res. 55 (7) (2019) 6109–6124, https://doi.org/10.1029/2018WR024404.
[45] M. Luhar, J. Rominger, H. Nepf, Interaction between flow, transport and vegetation spatial structure, Environ. Fluid Mech. 8 (5–6) (2001) 423–439, https://doi.org/10.1007/s10652-008-9080-9, 2008.
[46] S.H. Ensign, M.W. Doyle, In-Channel transient storage and associated nutrient Retention: evidence from experimental Manipulations, Limnol. Oceanogr. 50 (6) (2005) 1740–1751, https://doi.org/10.4319/lo.2005.50.6.1740.
[47] M. Salehin, A.I. Packman, A. Wörman, Comparison of transient storage in vegetated and unvegetated reaches of a small agricultural stream in Sweden: seasonal variation and anthropogenic manipulation, Adv. Water Resour. 26 (9) (2003) 951–964, https://doi.org/10.1016/S0309-1708(03)00084-8.
[48] G. Jin, S. Zhang, B. Zhou, Y. Yang, Z. Zhang, H. Chen, H. Tang, Solute transport characteristics in the streambed due to rigid non-submerged plants: experiment and simulations, J. Hydrol. 619 (2023) 129315, https://doi.org/10.1016/j.jhydrol.2023.129315.
[49] H.M. Nepf, E.W. Koch, Vertical secondary flows in submersed plant-like arrays, Limnol. Oceanogr. 44 (4) (1999) 1072–1080, https://doi.org/10.4319/lo.1999.44.4.1072.
[50] P. Lacoul, B. Freedman, Environmental influences on aquatic plants in freshwater ecosystems, Environ. Rev. 14 (2) (2006) 89–136, https://doi.org/10.1139/a06-001.
[51] Y. Zhang, E. Jeppesen, X. Liu, B. Qin, K. Shi, Y. Zhou, S.M. Thomaz, J. Deng, Global loss of aquatic vegetation in lakes, Earth Sci. Rev. 173 (2017) 259–265, https://doi.org/10.1016/j.earscirev.2017.08.013.
[52] C. Lønborg, A. Thomasberger, P.A.U. Stæhr, A. Stockmarr, S. Sengupta, M.L. Rasmussen, L.T. Nielsen, L.B. Hansen, K. Timmermann, Submerged aquatic vegetation: overview of monitoring techniques used for the identification and determination of spatial distribution in European coastal waters, Integrated Environ. Assess. Manag. 18 (4) (2022) 892–908, https://doi.org/10.1002/ieam.4552.
[53] W.-x. Huai, S. Li, G.G. Katul, M.-y. Liu, Z.-h. Yang, Flow dynamics and sediment transport in vegetated rivers: a review, Journal of hydrodynamics. Series B 33 (3) (2021) 400–420, https://doi.org/10.1007/s42241-021-0043-7.

[54] R.O. Tinoco, J.E. San Juan, J.C. Mullarney, Simplification bias; lessons from laboratory and field experiments on flow through aquatic vegetation, Earth Surf. Process. Landforms 45 (1) (2020) 121–143, https://doi.org/10.1002/esp.4743.
[55] J. Aberle, J. Järvelä, Flow resistance of emergent rigid and flexible floodplain vegetation, J. Hydraul. Res. 51 (1) (2013) 33–45, https://doi.org/10.1080/00221686.2012.754795.
[56] T. Zhao, H.M. Nepf, Turbulence Dictates bedload transport in vegetated channels without dependence on stem diameter and arrangement, Geophys. Res. Lett. 48 (21) (2021), https://doi.org/10.1029/2021GL095316 n/a.
[57] J.Q. Yang, F. Kerger, H.M. Nepf, Estimation of the bed shear stress in vegetated and bare channels with smooth beds, Water Resour. Res. 51 (5) (2015) 3647–3663, https://doi.org/10.1002/2014WR016042.
[58] C.-Y. Tseng, R.O. Tinoco, A two-layer turbulence-based model to predict suspended sediment concentration in flows with aquatic vegetation, Geophys. Res. Lett. 48 (3) (2021), https://doi.org/10.1029/2020GL091255 n/a.
[59] E.M. Yager, M.W. Schmeeckle, The influence of vegetation on turbulence and bed load transport, Jl of geophysical research. Earth surface 118 (3) (2013) 1585–1601, https://doi.org/10.1002/jgrf.20085.
[60] L. Zong, H. Nepf, Flow and deposition in and around a finite patch of vegetation, Geomorphology 116 (3) (2010) 363–372, https://doi.org/10.1016/j.geomorph.2009.11.020.
[61] Z. Chen, A. Ortiz, L. Zong, H. Nepf, The wake structure behind a porous obstruction and its implications for deposition near a finite patch of emergent vegetation, Water Resour. Res. 48 (9) (2012), https://doi.org/10.1029/2012WR012224 n/a.
[62] J.T. Rominger, H.M. Nepf, Flow adjustment and interior flow associated with a rectangular porous obstruction, J. Fluid Mech. 680 (2011) 636–659, https://doi.org/10.1017/jfm.2011.199.
[63] Y. Tanino, H.M. Nepf, Lateral dispersion in random cylinder arrays at high Reynolds number, J. Fluid Mech. 600 (2008) 339–371, https://doi.org/10.1017/S0022112008000505.
[64] P.W. Bearman, J.K. Harvey, Control of circular cylinder flow by the use of dimples, AIAA J. 31 (10) (1993) 1753–1756, https://doi.org/10.2514/3.11844.
[65] R.A. Antonia, S. Rajagopalan, Determination of drag of a circular cylinder, AIAA J. 28 (10) (1990) 1833–1834, https://doi.org/10.2514/3.10485.
[66] R.E.D. Bishop, A.Y. Hassan, The lift and drag forces on a circular cylinder in a flowing fluid, Proc. Roy. Soc. Lond. Math. Phys. Sci. 277 (1368) (1964) 32–50, https://doi.org/10.1098/rspa.1964.0004.
[67] U.C. Kothyari, K. Hayashi, H. Hashimoto, Drag coefficient of unsubmerged rigid vegetation stems in open channel flows, J. Hydraul. Res. 47 (6) (2009) 691–699, https://doi.org/10.3826/jhr.2009.3283.
[68] N.-S. Cheng, H.T. Nguyen, Hydraulic radius for evaluating resistance induced by simulated emergent vegetation in open-channel flows, J. Hydraul. Eng. 137 (9) (2011) 995–1004, https://doi.org/10.1061/(ASCE)HY.1943-7900.0000377.
[69] R.K. Jain, U.C. Kothyari, Cohesion influences on erosion and bed load transport: influence of COHESION, Water Resour. Res. 45 (6) (2009), https://doi.org/10.1029/2008WR007044.
[70] P.Y. Julien, Erosion and Sedimentation, Cambridge University Press, Cambridge, 2010.
[71] S. Petryk, Drag on Cylinders in Open Channel Flow, Colorado State University, 1969.
[72] D.L. Koch, A.J.C. Ladd, Moderate Reynolds number flows through periodic and random arrays of aligned cylinders, J. Fluid Mech. 349 (1997) 31–66, https://doi.org/10.1017/S002211209700671X.
[73] Y. Ishikawa, K. Mizuhara, M. Ashida, Drag Force on Multiple Rows of Cylinders in an Open Channel, Kyushu Univ, Fukuoka, Japan, 2000. *Grant-in-aid research project report*.
[74] A.M. Thompson, B.N. Wilson, T. Hustrulid, Instrumentation to measure drag on idealized vegetal elements in overland flow, Transactions of the ASAE 46 (2) (2003) 295–302, https://doi.org/10.13031/2013.12980.
[75] C.S. James, A.L. Birkhead, A.A. Jordanova, J.J. O'Sullivan, Flow resistance of emergent vegetation, J. Hydraul. Res. 42 (4) (2004) 390–398, https://doi.org/10.1080/00221686.2004.9641206.
[76] D. Liu, P. Diplas, J.D. Fairbanks, C.C. Hodges, An experimental study of flow through rigid vegetation, J. Geophys. Res. 113 (F4) (2008) F04015, https://doi.org/10.1029/2008JF001042 n/a.
[77] R.M. Ferreira, A.M. Ricardo, M.J. Franca, Discussion of "laboratory investigation of mean drag in a random array of rigid, emergent cylinders" by Yukie Tanino and Heidi M. Nepf, J. Hydraul. Eng. 134 (8) (2009) 690–693, https://doi.org/10.1061/(ASCE)HY.1943-7900.0000021.
[78] T. Stoesser, S.J. Kim, P. Diplas, Turbulent flow through idealized emergent vegetation, J. Hydraul. Eng. 136 (12) (2010) 1003–1017, https://doi.org/10.1061/(ASCE)HY.1943-7900.0000153.
[79] T.H. Von Karman, Mechanical Similitude and Turbulence, 1931. Legacy CDMS.
[80] V. Etminan Farooji, M. Ghisalberti, R.J. Lowe, Predicting bed shear stresses in vegetated channels, Water Resour. Res. 54 (11) (2018) 9187–9206, https://doi.org/10.1029/2018WR022811.
[81] M.R. Raupach, R.H. Shaw, Averaging procedures for flow within vegetation canopies, Boundary-Layer Meteorol. 22 (1) (1982) 79–90, https://doi.org/10.1007/BF00128057.
[82] H. Tennekes, J.L. Lumley, A First Course in Turbulence, MIT Press, 1972.
[83] J.Q. Yang, H. Chung, H.M. Nepf, The onset of sediment transport in vegetated channels predicted by turbulent kinetic energy, 11, Geophys. Res. Lett. 43 (21) (2016), https://doi.org/10.1002/2016GL071092, 261-211,268.
[84] Y. Xu, H. Nepf, Measured and predicted turbulent kinetic energy in flow through emergent vegetation with real plant morphology, Water Resour. Res. 56 (12) (2020), https://doi.org/10.1029/2020WR027892 n/a.
[85] K.R. Stapleton, D.A. Huntley, Seabed stress determinations using the inertial dissipation method and the turbulent kinetic energy method: Technical & software bulletin 1995, Earth Surf. Process. Landforms 20 (9) (1995) 807–815.
[86] B.L. White, H.M. Nepf, A vortex-based model of velocity and shear stress in a partially vegetated shallow channel, Water Resour. Res. 44 (1) (2008) W01412, https://doi.org/10.1029/2006WR005651 n/a.
[87] M. Ghisalberti, H.M. Nepf, Mixing layers and coherent structures in vegetated aquatic flows, J. Geophys. Res. 107 (C2) (2002), https://doi.org/10.1029/2001JC000871, 3-1-3-11.
[88] H. Nepf, M. Ghisalberti, Flow and transport in channels with submerged vegetation, Acta Geophys. 56 (3) (2008) 753–777, https://doi.org/10.2478/s11600-008-0017-y.
[89] M. Ghisalberti, H. Nepf, The structure of the shear layer in flows over rigid and flexible canopies, Environ. Fluid Mech. 6 (3) (2006) 277–301, https://doi.org/10.1007/s10652-006-0002-4. Dordrecht, Netherlands : 2001.
[90] D. Termini, Turbulent mixing and dispersion mechanisms over flexible and dense vegetation, Acta Geophys. 67 (3) (2019) 961–970, https://doi.org/10.1007/s11600-019-00272-8.
[91] A. Sukhodolov, T. Sukhodolova, J. Aberle, Modelling of flexible aquatic plants from silicone syntactic foams, J. Hydraul. Res. 60 (1) (2022) 173–181, https://doi.org/10.1080/00221686.2021.1903590.
[92] M. Luhar, H.M. Nepf, Flow-induced reconfiguration of buoyant and flexible aquatic vegetation, Limnol. Oceanogr. 56 (6) (2011) 2003–2017, https://doi.org/10.4319/lo.2011.56.6.2003.
[93] F. Sonnenwald, J.R. Hart, P. West, V.R. Stovin, I. Guymer, Transverse and longitudinal mixing in real emergent vegetation at low velocities, Water Resour. Res. 53 (1) (2017) 961–978, https://doi.org/10.1002/2016WR019937.
[94] G.I. Taylor, Dispersion of soluble matter in solvent flowing slowly through a tube, Proc. Roy. Soc. Lond. Math. Phys. Sci. 219 (1137) (1953) 186–203, https://doi.org/10.1098/rspa.1953.0139.
[95] Z. Wu, G.Q. Chen, Approach to transverse uniformity of concentration distribution of a solute in a solvent flowing along a straight pipe, J. Fluid Mech. 740 (2014) 196–213, https://doi.org/10.1017/jfm.2013.648.
[96] Y. Mazda, N. Kanazawa, T. Kurokawa, Dependence of dispersion on vegetation density in a tidal creek-mangrove swamp system, Mangroves Salt Marshes 3 (1) (1999) 59–66, https://doi.org/10.1023/A:1009929921740.
[97] B.L. White, H.M. Nepf, Scalar transport in random cylinder arrays at moderate Reynolds number, J. Fluid Mech. 487 (487) (2003) 43–79, https://doi.org/10.1017/S0022112003004579.
[98] E. Murphy, Longitudinal Dispersion in Vegetated Flow, Massachusetts Institute of Technology, 2006.
[99] E. Gacia, C.M. Duarte, Sediment Retention by a Mediterranean Posidonia oceanica Meadow: the balance between deposition and resuspension, Estuar. Coast Shelf Sci. 52 (4) (2001) 505–514, https://doi.org/10.1006/ecss.2000.0753.
[100] J.A. Cotton, G. Wharton, J.A.B. Bass, C.M. Heppell, R.S. Wotton, The effects of seasonal changes to in-stream vegetation cover on patterns of flow and accumulation of sediment, Geomorphology 77 (3–4) (2006) 320–334, https://doi.org/10.1016/j.geomorph.2006.01.010. Amsterdam, Netherlands.
[101] T.J. Bouma, L.A. van Duren, S. Temmerman, T. Claverie, A. Blanco-Garcia, T. Ysebaert, P.M.J. Herman, Spatial flow and sedimentation patterns within patches of epibenthic structures combining field, flume and modelling experiments, Continent. Shelf Res. 27 (8) (2007) 1020–1045, https://doi.org/10.1016/j.csr.2005.12.019.
[102] J.T. Rominger, A.F. Lightbody, H.M. Nepf, Effects of added vegetation on sand bar stability and stream hydrodynamics, J. Hydraul. Eng. 136 (12) (2010) 994–1002, https://doi.org/10.1061/(ASCE)HY.1943-7900.0000215.
[103] L. Zong, H. Nepf, Spatial distribution of deposition within a patch of vegetation, Water Resour. Res. 47 (3) (2011), https://doi.org/10.1029/2010WR009516 n/a.
[104] H.A. Einstein, A.G. Anderson, J.W. Johnson, Anonymous. A distinction between bed-load and suspended load in natural streams, Eos, Transactions American Geophysical Union 21 (2) (1940) 628–633, https://doi.org/10.1029/TR021i002p00628.
[105] H.S. Woo, P.Y. Julien, E.V. Richardson, Washload and fine sediment load, J. Hydraul. Eng. 112 (6) (1986) 541–545, https://doi.org/10.1061/(ASCE)0733-9429(1986)112:6(541).
[106] K. Ramos, S. Gibson, L.M. Kavvas, R. Heath, J. Sharp, Estimating bed-load advection and dispersion coefficients with the method of moments, in: World Environmental and Water Resources Congress, 2015, pp. 1736–1741, 2015.
[107] K. Waldschläger, M.Z.M. Brückner, B. Carney Almroth, C.R. Hackney, T.M. Adyel, O.S. Alimi, S.L. Belontz, W. Cowger, D. Doyle, A. Gray, et al., Learning from natural sediments to tackle microplastics challenges: a multidisciplinary perspective, Earth Sci. Rev. 228 (2022) 104021, https://doi.org/10.1016/j.earscirev.2022.104021.
[108] G. Stokes, On the effect of internal friction of fluids on the motion of pendulums, Trans. Camb. phi1. S0c 9 (8) (1850) 106.

[109] L.C. Van Rijn, Handbook Sediment Transport by Currents and Waves, Delft Hydraulics Laboratory, 1989.
[110] A.J. Raudkivi, Loose Boundary Hydraulics, Pergamon Press, 1967.
[111] J.S. McNown, J. Malaika, Effects of particle shape on settling velocity at low Reynolds numbers, Eos, Transactions American Geophysical Union 31 (1) (1950) 74–82, https://doi.org/10.1029/TR031i001p00074.
[112] R.I. Ferguson, M. Church, A simple universal equation for grain settling velocity, J. Sediment. Res. 74 (6) (2004) 933–937, https://doi.org/10.1306/051204740933.
[113] K. Kranck, Flocculation of suspended sediment in the Sea, Nature (London) 246 (5432) (1973) 348–350, https://doi.org/10.1038/246348a0.
[114] J. Gregory, C.R. O'Melia, Fundamentals of flocculation, Crit. Rev. Environ. Control 19 (3) (1989) 185–230, https://doi.org/10.1080/10643389809388365.
[115] A.W. Vreman, Turbulence attenuation in particle-laden flow in smooth and rough channels, J. Fluid Mech. 773 (2015) 103–136, https://doi.org/10.1017/jfm.2015.208.
[116] Y. Yao, C.S. Criddle, O.B. Fringer, The effects of particle clustering on hindered settling in high-concentration particle suspensions, J. Fluid Mech. 920 (2021), https://doi.org/10.1017/jfm.2021.470.
[117] H. Rouse, Experiments on the Mechanics of Sediment Suspension, 1939.
[118] D.A. Donzis, K. Aditya, K.R. Sreenivasan, P.K. Yeung, The turbulent Schmidt number, J. Fluid Eng. 136 (6) (2014) 60912, https://doi.org/10.1115/1.4026619.
[119] D.A. Shaw, T.J. Hanratty, Turbulent mass transfer rates to a wall for large Schmidt numbers, AIChE J. 23 (1) (1977) 28–37, https://doi.org/10.1002/aic.690230106.
[120] J. Fredsøe, Mechanics of Coastal Sediment Transport, 1992.
[121] B.P. Boudreau, P.S. Hill, Rouse revisited the bottom boundary condition for suspended sediment profiles, Mar. Geol. 419 (2020) 106066, https://doi.org/10.1016/j.margeo.2019.106066.
[122] T.-J. Hsu, J.T. Jenkins, P.L.F. Liu, On two-phase sediment transport dilute flow, J. Geophys. Res. 108 (C3) (2003) 3057–n/a, https://doi.org/10.1029/2001JC001276.
[123] F. Lopez, M. Garcia, Open-channel Flow through Simulated Vegetation : Turbulence Modeling and Sediment Transport, U.S. Army Engineer Waterways Experiment Station, 1997.
[124] S.R. Abt, W.P. Clary, C.I. Thornton, Sediment deposition and Entrapment in vegetated streambeds, J. Irrigat. Drain. Eng. 120 (6) (1994) 1098–1111, https://doi.org/10.1061/(ASCE)0733-9437(1994)120:6(1098).
[125] A. Defina, A.C. Bixio, Mean flow and turbulence in vegetated open channel flow, Water Resour. Res. 41 (7) (2005) W07006, https://doi.org/10.1029/2004WR003475 n/a.
[126] Y. Xu, H. Nepf, Suspended sediment concentration profile in a Typha latifolia canopy, Water Resour. Res. 57 (9) (2021), https://doi.org/10.1029/2021WR029902 n/a.
[127] J. Wingenroth, C. Yee, J. Nghiem, L. Larsen, Effects of stem density and Reynolds number on fine sediment interception by emergent vegetation, Geosciences 11 (3) (2021) 136, https://doi.org/10.3390/geosciences11030136.
[128] K.E. Fauria, R.E. Kerwin, D. Nover, S.G. Schladow, Suspended particle capture by synthetic vegetation in a laboratory flume, Water Resour. Res. 51 (11) (2015) 9112–9126, https://doi.org/10.1002/2014WR016481.
[129] A.H. Elliott, Settling of fine sediment in a channel with emergent vegetation, J. Hydraul. Eng. 126 (8) (2000) 570–577, https://doi.org/10.1061/(ASCE)0733-9429(2000)126:8(570).
[130] V. Verschoren, J. Schoelynck, T. Cox, K. Schoutens, S. Temmerman, P. Meire, Opposing effects of aquatic vegetation on hydraulic functioning and transport of dissolved and organic particulate matter in a lowland river: a field experiment, Ecol. Eng. 105 (2017) 221–230, https://doi.org/10.1016/j.ecoleng.2017.04.064.
[131] E.K. Owowenu, C.F. Nnadozie, F. Akamagwuna, X.S. Noundou, J.E. Uku, O.N. Odume, A critical review of environmental factors influencing the transport dynamics of microplastics in riverine systems: implications for ecological studies, Aquat. Ecol. 57 (2) (2023) 557–570, https://doi.org/10.1007/s10452-023-10029-7.
[132] M.T. Rose, A.N. Crossan, I.R. Kennedy, The effect of vegetation on pesticide dissipation from ponded treatment wetlands: Quantification using a simple model, Chemosphere 72 (7) (2008) 999–1005, https://doi.org/10.1016/j.chemosphere.2008.04.059.
[133] P. Peruzzo, A. Defina, H. Nepf, Capillary trapping of buoyant particles within regions of emergent vegetation, Water Resour. Res. 48 (7) (2012), https://doi.org/10.1029/2012WR011944 np-n/a.
[134] P.L. Lenaker, A.K. Baldwin, S.R. Corsi, S.A. Mason, P.C. Reneau, J.W. Scott, Vertical distribution of microplastics in the water column and Surficial sediment from the Milwaukee river basin to lake Michigan, Environmental science & technology 53 (21) (2019) 12227–12237, https://doi.org/10.1021/acs.est.9b03850.
[135] M.R. Palmer, H.M. Nepf, J.R.P. Thomas, J.D. Ackerman, Observations of particle capture on a cylindrical Collector: implications for particle accumulation and Removal in aquatic systems, Limnol. Oceanogr. 49 (1) (2004) 76–85, https://doi.org/10.4319/lo.2004.49.1.0076.
[136] A. Defina, P. Peruzzo, Floating particle trapping and diffusion in vegetated open channel flow: floating particle diffusion in vegetated flow, Water Resour. Res. 46 (11) (2010), https://doi.org/10.1029/2010WR009353.
[137] B. Gomez, Bedload transport, Earth Sci. Rev. 31 (2) (1991) 89–132.
[138] A. Shields, Anwendung der Aehnlichkeitsmechanik und der Turbulenzforschung auf die Geschiebebewegung, PhD Thesis Technical University, Berlin, 1936.
[139] J.M. Buffington, D.R. Montgomery, Effects of hydraulic roughness on surface textures of gravel-bed rivers, Water Resour. Res. 35 (11) (1999) 3507–3521, https://doi.org/10.1029/1999WR900138.
[140] P.R. Wilcock, Sediment Transport Primer : Estimating Bed-Material Transport in Gravel-Bed Rivers, 2009.
[141] W.R. Brownlie, Flow depth in sand-bed channels, J. Hydraul. Eng. 109 (7) (1983) 959–990, https://doi.org/10.1061/(ASCE)0733-9429(1983)109:7(959).
[142] Z. Cao, G. Pender, J. Meng, Explicit formulation of the shields diagram for incipient motion of sediment, J. Hydraul. Eng. 132 (10) (2006) 1097–1099, https://doi.org/10.1061/(ASCE)0733-9429(2006)132:10(1097).
[143] P.R. Wilcock, Critical shear stress of natural sediments, J. Hydraul. Eng. 119 (4) (1993) 491–505, https://doi.org/10.1061/(ASCE)0733-9429(1993)119:4(491).
[144] W. Lick, L. Lin, J. Gailani, Initiation of movement of quartz particles, J. Hydraul. Eng. 130 (8) (2004) 755–761, https://doi.org/10.1061/(ASCE)0733-9429(2004)130:8(755).
[145] P.R. Wilcock, J.C. Crowe, Surface-based transport model for mixed-size sediment, J. Hydraul. Eng. 129 (2) (2003) 120–128, https://doi.org/10.1061/(ASCE)0733-9429(2003)129:2(120).
[146] G. Proffitt, A. Sutherland, Transport of non-uniform sediments, J. Hydraul. Res. 21 (1) (1983) 33–43.
[147] G. Parker, A.J. Sutherland, Fluvial armor, J. Hydraul. Res. 28 (5) (1990) 529–544, https://doi.org/10.1080/00221689009499044.
[148] M.P. Lamb, W.E. Dietrich, J.G. Venditti, Is the critical shields stress for incipient sediment motion dependent on channel-bed slope? J. Geophys. Res. 113 (F2) (2008) F02008, https://doi.org/10.1029/2007JF000831.
[149] J.S. Scheingross, E.W. Winchell, M.P. Lamb, W.E. Dietrich, Influence of bed patchiness, slope, grain hiding, and form drag on gravel mobilization in very steep streams, Jl of geophysical research. Earth surface 118 (2) (2013) 982–1001, https://doi.org/10.1002/jgrf.20067.
[150] J.W. Kirchner, W.E. Dietrich, F. Iseya, H. Ikeda, The variability of critical shear stress, friction angle, and grain protrusion in water-worked sediments, Sedimentology 37 (4) (1990) 647–672, https://doi.org/10.1111/j.1365-3091.1990.tb00627.x.
[151] F. Charru, H. Mouilleron, O. Eiff, Erosion and deposition of particles on a bed sheared by a viscous flow, J. Fluid Mech. 519 (2004) 55–80, https://doi.org/10.1017/S0022112004001028.
[152] C.C. Masteller, N.J. Finnegan, J.M. Turowski, E.M. Yager, D. Rickenmann, History-dependent threshold for motion revealed by continuous bedload transport measurements in a steep mountain stream, Geophys. Res. Lett. 46 (5) (2019) 2583–2591, https://doi.org/10.1029/2018GL081325.
[153] M. du Boys, Étude du régime du Rhône et de l'action exercée par les eaux sur un lit à fond de graviers indéfiniment affouillable. vol. 18 of 5, in: Annales des Ponts et Chaussées, 1879.
[154] R.A. Bagnold, Transport of solids by natural water flow: evidence for a worldwide correlation, Proc. Roy. Soc. Lond. Math. Phys. Sci. 405 (1829) (1986) 369–374, https://doi.org/10.1098/rspa.1986.0059.
[155] E. Meyer-Peter, R. Müller, Formulas for bed-load transport, in: IAHSR 2nd Meeting, Stockholm, Appendix, 2, IAHR, 1948.
[156] M. Wong, G. Parker, P. DeVries, T.M. Brown, S.J. Burges, Experiments on dispersion of tracer stones under lower-regime plane-bed equilibrium bed load transport, Water Resour. Res. 43 (3) (2007) W03440, https://doi.org/10.1029/2006WR005172, n/a.
[157] H.A. Einstein, The Bed-Load Function for Sediment Transportation in Open Channel Flows, US Department of Agriculture, 1950.
[158] C.B. Brown, Sediment transportation, Engineering hydraulics 12 (1950) 769–857.
[159] C. Ancey, Bedload transport: a walk between randomness and determinism. Part 1. The state of the art, J. Hydraul. Res. 58 (1) (2020) 1–17, https://doi.org/10.1080/00221686.2019.1702594.
[160] M. Wong, G. Parker, Reanalysis and Correction of bed-load relation of Meyer-Peter and Müller using their Own Database, J. Hydraul. Eng. 132 (11) (2006) 1159–1168, https://doi.org/10.1061/(ASCE)0733-9429(2006)132:11(1159).
[161] D.J. Furbish, P.K. Haff, J.C. Roseberry, M.W. Schmeeckle, A probabilistic description of the bed load sediment flux: 1. Theory, J. Geophys. Res.: Earth Surf. 117 (F3) (2012), https://doi.org/10.1029/2012JF002352 n/a.
[162] D.J. Furbish, A.E. Ball, M.W. Schmeeckle, A probabilistic description of the bed load sediment flux: 4. Fickian diffusion at low transport rates, J. Geophys. Res.: Earth Surf. 117 (F3) (2012), https://doi.org/10.1029/2012JF002356 n/a.
[163] P. Bohorquez, C. Ancey, Stochastic-deterministic modeling of bed load transport in shallow water flow over erodible slope linear stability analysis and numerical simulation, Adv. Water Resour. 83 (2015) 36–54, https://doi.org/10.1016/j.advwatres.2015.05.016.
[164] Z. Wu, A. Singh, E. Foufoula-Georgiou, M. Guala, X. Fu, G. Wang, A velocity-variation-based formulation for bedload particle hops in rivers, J. Fluid Mech. 912 (2021), https://doi.org/10.1017/jfm.2020.1126.
[165] Z. Wu, W. Jiang, L. Zeng, X. Fu, Theoretical analysis for bedload particle deposition and hop statistics, J. Fluid Mech. 954 (2023), https://doi.org/10.1017/jfm.2022.959.
[166] J.C. Winterwerp, Introduction to the Physics of Cohesive Sediment in the

Marine Environment, Elsevier, Amsterdam, 2004.
[167] C. Ancey, Bedload transport: a walk between randomness and determinism. Part 2. Challenges and prospects, J. Hydraul. Res. 58 (1) (2020) 18–33, https://doi.org/10.1080/00221686.2019.1702595.
[168] W.H. Hager, Bed-load transport: advances up to 1945 and outlook into the future, J. Hydraul. Res. 56 (5) (2018) 596–607, https://doi.org/10.1080/00221686.2017.1405370.
[169] J.G. Herbertson, A critical review of conventional bed load formulae, J. Hydrol. 8 (1) (1969) 1–25, https://doi.org/10.1016/0022-1694(69)90028-6.
[170] A.A. Jordanova, C.S. James, Experimental study of bed load transport through emergent vegetation, J. Hydraul. Eng. 129 (6) (2003) 474–478, https://doi.org/10.1061/(ASCE)0733-9429(2003)129:6(474).
[171] W. Weiming, H. Zhiguo, Effects of vegetation on flow conveyance and sediment transport capacity, Int. J. Sediment Res. 24 (3) (2009) 247–259.
[172] T. Hongwu, H. Wang, D. Liang, S. Lv, L. Yan, Incipient motion of sediment in the presence of emergent rigid vegetation, Journal of Hydro-Environment Research 7 (3) (2013) 202–208.
[173] J. Widdows, N.D. Pope, M.D. Brinsley, Effect of Spartina anglica stems on near-bed hydrodynamics, sediment erodability and morphological changes on an intertidal mudflat, Mar. Ecol. Prog. Ser. 362 (2008) 45–57, https://doi.org/10.3354/meps07448.
[174] N.-S. Cheng, M. Wei, Y. Lu, Critical flow velocity for incipient sediment motion in open channel flow with rigid emergent vegetation, J. Eng. Mech. 146 (11) (2020), https://doi.org/10.1061/(ASCE)EM.1943-7889.0001857.
[175] H. Wu, N. Cheng, Y.-M. Chiew, Bed-load transport in vegetated flows; phenomena, parametrization, and prediction, Water Resour. Res. 57 (4) (2021), https://doi.org/10.1029/2020WR028143 n/a.
[176] H. Zhang, Transport of microplastics in coastal seas, Estuar. Coast Shelf Sci. 199 (2017) 74–86, https://doi.org/10.1016/j.ecss.2017.09.032.
[177] A. Krajewski, A. Hejduk, L. Hejduk, First evidence of microplastic presence in bed load sediments of a small urban stream in Warsaw, Sustainability 14 (23) (2022) 16017, https://doi.org/10.3390/su142316017.
[178] V. Yadav, M. Sherly, P. Ranjan, R.O. Tinoco, A. Boldrin, A. Damgaard, A. Laurent, Framework for quantifying environmental losses of plastics from landfills, Resour. Conserv. Recycl. 161 (2020) 104914.
[179] K. Waldschlaeger, H. Schuettrumpf, Erosion Behavior of different microplastic particles in comparison to natural sediments, Environmental science & technology 53 (22) (2019) 13219–13227, https://doi.org/10.1021/acs.est.9b05394.
[180] A. Armanini, V. Cavedon, Bed-load through emergent vegetation, Adv. Water Resour. 129 (2019) 250–259, https://doi.org/10.1016/j.advwatres.2019.05.021.
[181] Y. Lu, N.-S. Cheng, M. Wei, Formulation of bed shear stress for computing bed-load transport rate in vegetated flows, Phys. Fluid. 33 (11) (1994), https://doi.org/10.1063/5.0067851, 2021.
[182] X. Wang, C. Gualtieri, W. Huai, Grain shear stress and bed-load transport in open channel flow with emergent vegetation, J. Hydrol. 618 (2023) 129204, https://doi.org/10.1016/j.jhydrol.2023.129204.
[183] D. Tonina, interaction: the hyporheic exchange, Fluid mechanics of environmental interfaces 255 (2012).
[184] K.R. Roche, G. Blois, J.L. Best, K.T. Christensen, A.F. Aubeneau, A.I. Packman, Turbulence Links momentum and solute exchange in coarse-Grained streambeds, Water Resour. Res. 54 (5) (2018) 3225–3242, https://doi.org/10.1029/2017WR021992.
[185] G. Rousseau, C. Ancey, Scanning PIV of turbulent flows over and through rough porous beds using refractive index matching, Exp. Fluid 61 (8) (2020), https://doi.org/10.1007/s00348-020-02990-y.
[186] J.J. Voermans, M. Ghisalberti, G.N. Ivey, A model for mass transport across the sediment-water interface, Water Resour. Res. 54 (4) (2018) 2799–2812, https://doi.org/10.1002/2017WR022418.
[187] Y. Yuan, X. Chen, M.B. Cardenas, X. Liu, L. Chen, Hyporheic exchange driven by submerged rigid vegetation: a modeling study, Water Resour. Res. 57 (6) (2021), https://doi.org/10.1029/2019WR026675 n/a.
[188] C.Y. Tseng, R.O. Tinoco, From Substrate to surface: a turbulence-based model for gas transfer across sediment-water-air interfaces in vegetated streams, Water Resour. Res. 58 (1) (2022), https://doi.org/10.1029/2021WR030776 n/a.
[189] E.M. Follett, H.M. Nepf, Sediment patterns near a model patch of reedy emergent vegetation, Geomorphology 179 (2012) 141–151, https://doi.org/10.1016/j.geomorph.2012.08.006.
[190] C. Le Bouteiller, J.G. Venditti, Vegetation-driven morphodynamic adjustments of a sand bed, Geophys. Res. Lett. 41 (11) (2014) 3876–3883, https://doi.org/10.1002/2014GL060155.
[191] K. Vastila, J. Jarvela, J. Aberle, Characteristic reference areas for estimating flow resistance of natural foliated vegetation, J. Hydrol. 492 (2013) 49–60, https://doi.org/10.1016/j.jhydrol.2013.04.015.
[192] V. Nikora, S. Larned, N. Nikora, K. Debnath, G. Cooper, M. Reid, Hydraulic resistance due to aquatic vegetation in small streams: field study, J. Hydraul. Eng. 134 (9) (2008) 1326–1332, https://doi.org/10.1061/(ASCE)0733-9429(2008)134:9(1326).
[193] D. Li, Z. Yang, Z. Sun, W. Huai, J. Liu, Theoretical model of suspended sediment concentration in a flow with submerged vegetation, Water 10 (11) (2018) 1656, https://doi.org/10.3390/w10111656.
[194] E. Follett, M. Chamecki, H. Nepf, Evaluation of a random displacement model for predicting particle escape from canopies using a simple eddy diffusivity model, Agric. For. Meteorol. 224 (2016) 40–48, https://doi.org/10.1016/j.agrformet.2016.04.004.
[195] Y. Li, L. Xie, T.C. Su, Profile of suspended sediment concentration in submerged vegetated shallow water flow, Water Resour. Res. 56 (4) (2020), https://doi.org/10.1029/2019WR025551 n/a.
[196] Z. Wu, G.Q. Chen, L. Zeng, Environmental dispersion in a two-zone wetland, Ecol. Model. 222 (3) (2011) 456–474, https://doi.org/10.1016/j.ecolmodel.2010.10.026.
[197] M.J. Baptist, A flume experiment on sediment transport with flexible, submerged vegetation, in: International Workshop on Riparian Forest Vegetated Channels: Hydraulic, Morphological and Ecological Aspects, RIPFOR, Trento, Italy, 2003.
[198] H. Wang, H.-w. Tang, H.-q. Zhao, X.-y. Zhao, S.-q. Lü, Incipient motion of sediment in presence of submerged flexible vegetation, Water Sci. Eng. 8 (1) (2015) 63–67, https://doi.org/10.1016/j.wse.2015.01.002.
[199] W. Vannoppen, M. Vanmaercke, S. de Baets, J. Poesen, A review of the mechanical effects of plant roots on concentrated flow erosion rates, Earth Sci. Rev. 150 (2015) 666–678, https://doi.org/10.1016/j.earscirev.2015.08.011.
[200] W. Vannoppen, J. Poesen, P. Peeters, S. de Baets, B. Vandevoorde, Root properties of vegetation communities and their impact on the erosion resistance of river dikes, Earth Surf. Process. Landforms 41 (14) (2016) 2038–2046, https://doi.org/10.1002/esp.3970.
[201] Y. Liu, L. Gong, X. Mu, Z. Zhang, T. Zhou, S. Zhang, Characterization and co-occurrence of microbial community in epiphytic biofilms and surface sediments of wetlands with submersed macrophytes, The Science of the total environment 715 (2020), https://doi.org/10.1016/j.scitotenv.2020.136950, 136950-136950.
[202] N. Gordon-Bradley, D.S. Lymperopoulou, H.N. Williams, Differences in bacterial community structure on Hydrilla verticillata and Vallisneria americana in a freshwater spring, Microb. Environ. 29 (1) (2014) 67–73, https://doi.org/10.1264/jsme2.ME13064.
[203] S.U. Gerbersdorf, K. Koca, D. de Beer, A. Chennu, C. Noss, U. Risse-Buhl, M. Weitere, O. Eiff, M. Wagner, J. Aberle, et al., Exploring flow-biofilm-sediment interactions: Assessment of current status and future challenges, Water Res. 185 (2020), https://doi.org/10.1016/j.watres.2020.116182, 116182-116182.
[204] Y. Wu, J. Liu, E.R. Rene, Periphytic biofilms: a promising nutrient utilization regulator in wetlands, Bioresour. Technol. 248 (Pt B) (2018) 44–48, https://doi.org/10.1016/j.biortech.2017.07.081.
[205] A. Caruso, F. Boano, L. Ridolfi, D.L. Chopp, A. Packman, Biofilm-induced bioclogging produces sharp interfaces in hyporheic flow, redox conditions, andmicrobial community structure, Geophys. Res. Lett. 44 (10) (2017) 4917–4925, https://doi.org/10.1002/2017GL073651.
[206] X. Zhang, N. Leonardi, C. Donatelli, S. Fagherazzi, Fate of cohesive sediments in a marsh-dominated estuary, Adv. Water Resour. 125 (2019) 32–40, https://doi.org/10.1016/j.advwatres.2019.01.003.
[207] D. Liang, X. Wang, B.N. Bockelmann-Evans, R.A. Falconer, Study on nutrient distribution and interaction with sediments in a macro-tidal estuary, Adv. Water Resour. 52 (2013) 207–220, https://doi.org/10.1016/j.advwatres.2012.11.015.
[208] W. Jiang, L. Zeng, X. Fu, Z. Wu, Analytical solutions for reactive shear dispersion with boundary adsorption and desorption, J. Fluid Mech. 947 (2022), https://doi.org/10.1017/jfm.2022.656.
[209] S. Shrivastava, M.J. Stewardson, M. Arora, Distribution of clay-sized sediments in streambeds and influence of fine sediment clogging on hyporheic exchange, Hydrol. Process. 34 (26) (2020) 5674–5685, https://doi.org/10.1002/hyp.13988.